Rolling Contact Fatigue

R. Ahmed, Heriot-Watt University (United Kingdom)

A MAJOR CAUSE of failure in components subjected to rolling or rolling/sliding contacts (e.g., rolling-contact bearings, gears, and cam/tappet arrangements) is contact fatigue. Rolling-contact fatigue (RCF) can be defined as the mechanism of crack propagation caused by the near-surface alternating stress field within the rolling-contact bodies, which eventually leads to material removal. The mechanism of RCF thus differs from the delamination theory of wear (Ref 1, 2), which also relies on cyclic loading but in sliding conditions and at asperity level. The alternating stress field in RCF is either in pure rolling (e.g., rolling-element bearings), or in rolling/sliding conditions (e.g., gear-tooth loading), depending on the absence or presence of gross sliding within the rolling-contact region. Microslip (e.g., Heathcote or Reynolds slip [Ref 3]) within the contact region is, however, inevitable in both pure rolling and rolling/sliding conditions. The term "RCF" in this article, however, refers to pure rolling configurations, except where specific references to rolling/sliding conditions are made.

The material removal in a RCF failure varies from micropitting, macropitting and spalling (Ref 4–5) in conventional bearing steels (Fig. 1) to delamination in hybrid ceramics (Ref 6) and overlay coatings (Ref 7), as discussed later. Contact geometry of the bodies subjected to RCF can be conforming (e.g., contact between the outer race and roller in a rolling-element roller bearing) or nonconforming (e.g., contact between the inner race and roller in a rolling-element roller bearing). The alternating stress field responsible for RCF failure can generally be idealized from Hertzian contact conditions in conventional metallic and ceramic materials (e.g., bearing steel and, Si_3N_4 ceramics), but the interpretation of stress fields needs to be cautiously approached when dealing with layered surfaces (e.g., overlay coatings). The preliminary focus in this article is on RCF of coated surfaces, although the stress field conditions are briefly reviewed for the RCF of a homogenous material surface.

Prediction of statistical fatigue life (Ref 8–10) and failure modes (Ref 4, 11–17) during RCF in conventional bearing steels also has been the focus of hundreds of papers and numerous books (Ref 18–20) in published literature. The scope of this article focuses principally on the RCF performance and failure modes of overlay coatings, such as those deposited by physical vapor deposition, chemical vapor deposition, and thermal spraying. Some background description of RCF in bearing steels is, however, useful and necessary, because RCF of steels is important. General background on RCF in bearing steels also helps develop an understanding of failure modes in overlay coatings discussed in this article. More detailed description of RCF in conventional bearing steels can be seen elsewhere (e.g., Ref 11–17), along with a general discussion of contact fatigue in the article "Fatigue Failures" in this Volume.

General Principles of RCF

General Background. The origin of RCF failure is understood to be stress concentrations, which initiate and propagate fatigue crack under cyclic loading. These stress concentrations occur due to surface or subsurface stress risers or to the geometry and kinematics of the contacting pair. Figure 2 summarizes a list of these stress risers, which have been the subject of numerous scientific investigations that have resulted in the improved life of rolling-element bearings (Ref 11). With the introduction of cleaner steels and greater precision in the manufacture of bearings, most of the surface and subsurface stress risers listed in Fig. 2 have been addressed. Nevertheless, the demand to operate rolling-element bearings in harsh tribological environments of lubrication, load, contamination, and temperature push for higher fatigue limits, and thus call for improved understanding of the RCF failure modes.

Four distinct failure modes have been established in rolling-contact bearings (Ref 5). These classifications include wear-type failures, plastic flow, contact fatigue, and bulk failures. Although the aim of this article is to comprehend RCF failures, wear-type failures that include surface removal and material transfer do not form a part of this background; Blau (Ref 13) has given a detailed account of rolling-contact wear (RCW), and he differentiates between RCF and RCW in the sense that RCF is a damage accumulation process under cyclic loading, whereas, RCW can be thought of as nucleation sites for initiating fatigue damage. Rolling-contact wear is thus critical in components operating in rolling-sliding contact (e.g., gears where the lubrication regime is either boundary or mixed). However, the full film lubrication generally seen in rolling-element bearings should prevent such damage, except at the start/stop of rolling motion. Similarly, plastic flow and bulk failure depend on the bulk thermal and mechanical properties of the bearing materials and can lead to permanent dimensional changes.

The most classical failure mode in rolling-contact components is RCF. Rolling-contact fatigue failure modes have previously been clas-

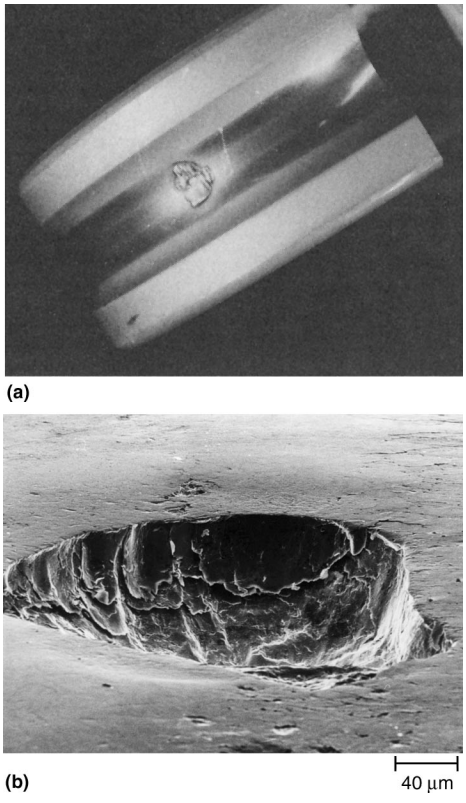

Fig. 1 Typical morphology of fatigue spall in rolling-element bearings. (a) Fatigue spall centered on a ball bearing raceway. (b) Fatigue spall on 12.7 mm (0.5 in.) diameter steel ball obtained using rolling four-ball machine

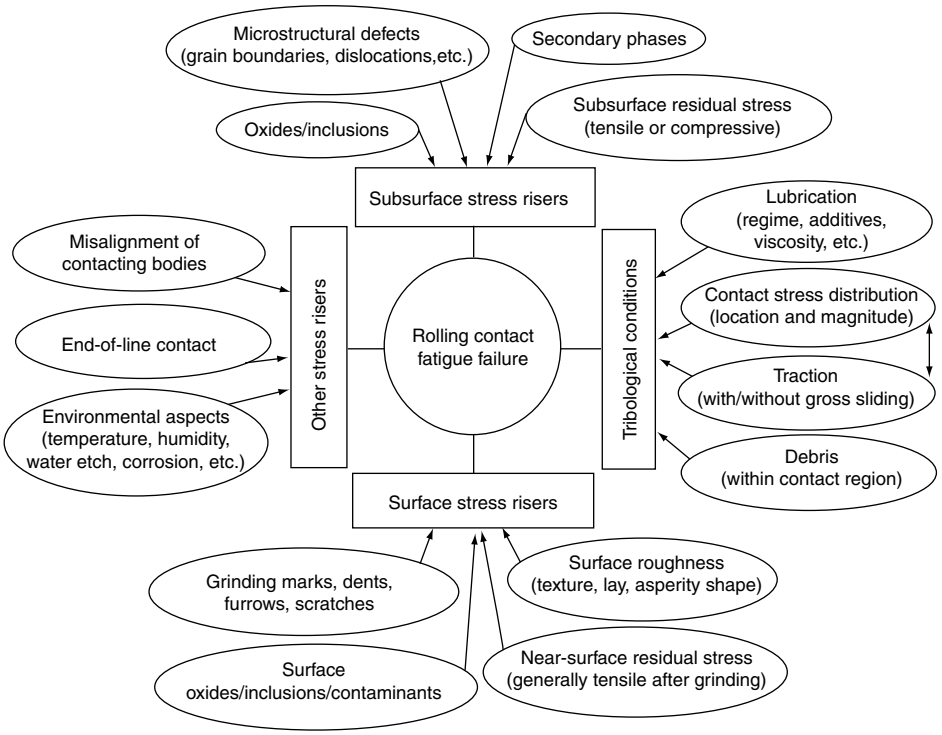

Fig. 2 Stress risers initiating rolling-contact fatigue failure

sified as pitting, case crushing, peeling, frosting, glazing, surface distress, and so on (Ref 15–17, 21, 22). Some of these terminologies are similar; for example, pitting and spalling are often used interchangeably in the European literature (Fig. 1). Littmann (Ref 17) has given an account of the contact fatigue damage classification system, and he identified six modes of fatigue failure—inclusion origin, subcase fatigue, surface origin, geometric stress concentrations, peeling, and section failure. Later studies classified these failure modes as surface originated and subsurface originated (23, 24). A more comprehensive classification of these failure modes can be found in Ref 25.

Regardless of the classification system used to categorize failure modes, the mechanism of RCF failure generally involves the following characteristics:

- Stress concentrations either at the surface or subsurface (Fig. 2)
- Crack initiation either at the surface or subsurface due to stress concentrations
- Crack propagation due to cyclic loading
- Spalling or pitting leading to debris
- Postfailure damage due to misalignment or debris within the contact region

The exact mode of fatigue failure can substantially vary from failure to failure, and a number of failure modes compete to reduce the overall life of rolling bearings. This is mainly due to the synergetic effect of competing failure modes in which both surface and subsurface origins of crack initiation and propagation can be significantly affected by tribological conditions. Additional factors, such as the role of residual stress; hydraulic pressure propagation, coupled with the shape, size, and location of individual surface or subsurface defects; and variations in tribological conditions within the contact region, thus present a complex interdependency.

Characteristics of RCF in Steel.* The stress condition associated with RCF is illustrated schematically in Fig. 3. With any condition of rolling, the maximum stress being applied at or very near the contact area is the shear stress parallel to the rolling surface at some point below the surface. For normally loaded gear teeth, this distance is from 0.18 to 0.30 mm (0.007 to 0.012 in.) below the surface just ahead of the rolling point of contact. If sliding is occurring in the same direction, the shear stress increases at the same point. If the shear plane is close to the surface, then light pitting can occur. If the shear plane is deep due to a heavy rolling-load contact, then the tendency is for the crack propagation to turn inward (Fig. 4). The cracks continue to propagate under repeated stress until heavy pitting or spalling takes place (Fig. 5).

There is always one characteristic (and often two) of RCF that will distinguishes it from other modes of surface-contact fatigue. Both characteristics can be observed only by an examination of the microstructure. In rolling contact, the surface will does not show a catastrophic movement; it remains as the original structure. For example, an unetched, polished sample taken near the origin of a subsurface fatigue crack (Fig. 6) very clearly shows undisturbed black oxides at the surface. The subsurface cracking could not have been caused by either abrasive or adhesive contact; it had to be by rolling. This is always the first evidence to look for when determining the type of applied stress.

*This section was adapted from L.E. Alban, Failures of Gears, *Failure Analysis and Prevention,* Vol 11 in *ASM Handbook,* 1986, p 593–594.

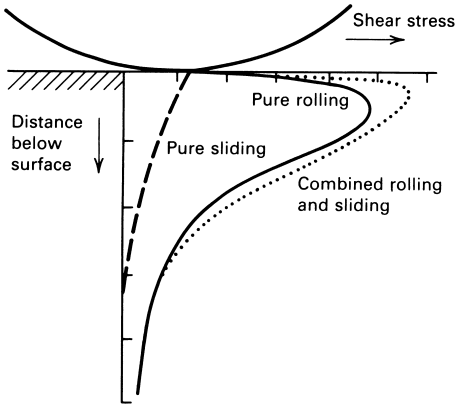

Fig. 3 Stress distribution in contacting surfaces due to rolling, sliding, and combined effect

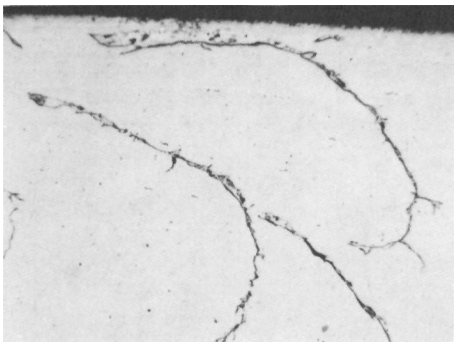

Fig. 4 Gear-tooth section. Rolling-contact fatigue. Crack origin subsurface. Progression was parallel to surface and inward away from surface. Not etched. 60×

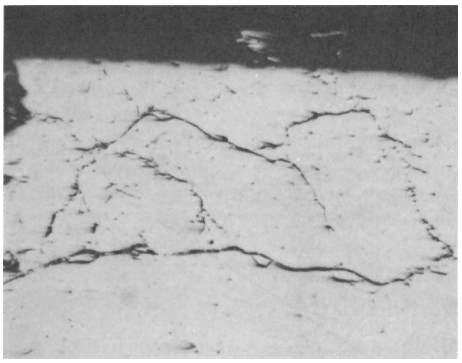

Fig. 5 Gear-tooth section. Rolling-contact fatigue. Crack origin subsurface. Progression was parallel with surface, inward, and finally to the surface to form a large pit or spall. Not etched. 60×

The second characteristic is common only in a martensitic steel that contains very little or no austenite and is found only at, along, or in line with the shear plane. This is a microstructural feature that has been termed "butterfly wings." If the sample in Fig. 6 is etched properly with 3% nital, the result is the microstructure shown in Fig. 7(a). Increasing the magnification to 310× shows more detail (Fig. 7b). This type of microstructural alteration is typically associated with an inclusion present, but not always. Extensive and very detailed studies of RCF refer to the gray substructure as white bands of altered martensite. It is believed that these substructures are caused when, under an extreme shearing stress, movement is called for but is restrained and contained to such an extent that the energy absorbed institutes a change in the microstructure ahead of a progressing crack. They are never observed when significant amounts of austenite are present; austenite quickly absorbs the energy and is converted to untempered martensite. They are also in an area that has not been deformed but has definitely been transformed. Each area has distinct boundaries, and the oncoming cracks appear to follow these boundaries. It has been noted that some academic studies refer to this same structure as being a transformed shear band product formed by adiabatic shear. A more detailed review of microstructural change in contact fatigue of steel is provided in the article "Contact Fatigue of Hardened Steel" in *ASM Handbook,* Volume 19, *Fatigue and Fracture* (Ref 11).

Rolling-Contact Fatigue Testing. The aforementioned complexity in underpinning the exact failure mechanism has led to simplified experimental contact model configurations (RCF tribometers), which have been extensively used to investigate the influence of changes in bearing materials, residual stress, and tribological conditions. Although the correlation between the fatigue life of these model contact configurations and the actual life of bearings in service has not been satisfactorily achieved, these RCF tribometers serve three important functions:

- They provide a method to benchmark the performance of existing and new generation of bearing materials prior to full-scale testing.
- They provide an insight to the mechanisms of individual failure modes by allowing the flexibility to vary individual parameters, such as lubrication, material cleanliness, contact load, surface roughness, and so on.
- Progressive tests allow the possibility to catalog the history of specific failures, thereby indicating the boundaries of failure initiation and propagation either in terms of progressive failure morphology or vibration levels, which can be useful for condition monitoring and wear mapping.

Although the failure mode depends on the tribological conditions selected for individual investigation, some test conditions adopted in RCF tribometers can accelerate the RCF failure, for example, by either increased contact loading or increased rolling velocity. This alters the elastic/plastic (shakedown) response, lubrication regime, and kinematics within the contact region when compared with those in the actual rolling-contact bearings. These variations can thus influence the mechanism of fatigue failure, and results of such investigations need to be interpreted in accordance with the adapted test conditions. Various researchers have compared the underpinning failure mechanisms observed during accelerated testing versus field performance. The influence of higher contact pressure on the residual stress profile and changes in white bands are considered in Ref 26. The elastic plastic shakedown can be thought responsible for changes that influences both the microstructure and also residual stress profile. Results have indicated that martensitic decay is possible for long duration tests and high toughness of bearing material of acceptable hardness leads to high RCF life in both accelerated and field tests.

The correct choice of tribometer is also critical for a given application. For example, a four-ball machine can simulate the kinematics of a deep-groove rolling-element ball bearing; however, the model contact in this tribometer considers a nonconforming contact between the inner race and rolling-element ball, which is not the case in an actual bearing. The capabilities of various RCF testing methods have been tabulated (Table 1) to compare the features of 13 different RCF tribometers (Ref 13). These tribometers (Ref 26, 27) have the capability to vary tribological conditions, for example, lubrication regime, contact configuration, and roll-to-slip ratio to mimic pure rolling or rolling/sliding motion for various rolling-contact applications. Even within a given category of RCF testers, there are generally numerous combinations of test configurations to allow the flexibility in experimental design; for example, in a rolling four-ball tester, there are numerous configurations (type I, II, III) possible to vary ball kinematics (Ref 28). Another modification to RCF testing has been the investigations of artificially induced surface defects (Ref 29, 30), which are thought to act as crack initiation sites during the RCF failure. Such investigations are useful in understanding the influence of surface defects on RCF failure and may also reduce the RCF testing time; the relevance of such investigations to the tribological conditions and failure modes in real bearing applications, however, requires a careful consideration of the differences in tribological conditions between them.

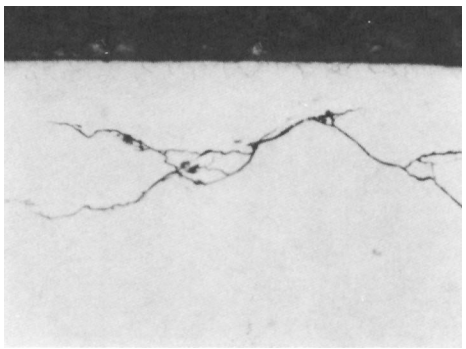

Fig. 6 Gear-tooth section. Rolling-contact fatigue distinguished by subsurface shear parallel to surface. Note the undisturbed black oxides at the surface, indicating no surface-material movement. Not etched. 125×

Theories of RCF Failure. The exact mechanism of RCF failure in engineering components needs to be appreciated in view of tribological conditions and various crack initiation and propagation sites; nevertheless, various theories (discussed subsequently) linking the location and magnitude of cyclic tensile or shear stress components to RCF failure are useful in understanding the failure mechanism. Although such theories based on cyclic stress components of the Hertzian stress field can sometimes oversimplify the RCF failure mechanism, the microscopic investigations comparing the cyclic stress components to RCF failure are compelling. For example, the existence of subsurface etchings and butterflies have been related to shear stress components under the contact surface (Ref 5, 11, 14, 15, 17).

Figure 8 illustrates a two-dimensional schematic of the location and magnitude of maximum shear (τ_{max}), orthogonal shear (q_{orth}) and maximum tensile (T_{max}) stress for a circular, dry-rolling frictionless contact. The contact diameter is assumed to be $2a$, and τ_{max} has a maximum value vertically below the center of contact region in a plane inclined at 45° to the coordinate axis (Ref 11). Its magnitude at any point can be calculated using the equation:

$$\tau_{max} = (\sigma_1 - \sigma_3)/2 = 0.35P_o \quad \text{(Eq 1)}$$

where σ_1 and σ_3 are the values of maximum and minimum principal stress, respectively, and P_o is

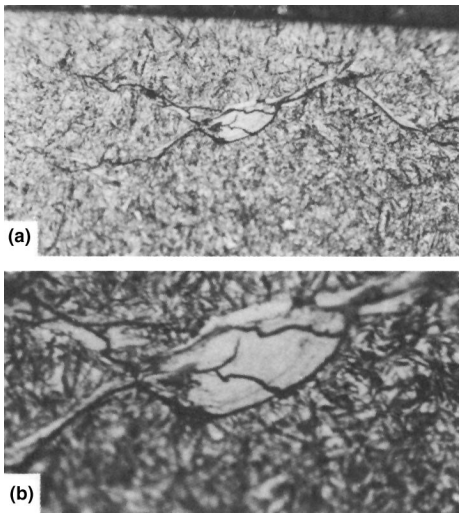

Fig. 7 Same sample as in Fig. 6, showing details of submicrostructure called butterfly wings. 3% nital etch. (a) 125×. (b) 310×

the peak compressive stress (Hertzian stress). Similarly, the orthogonal shear stress (q_{orth}) acts on planes parallel and perpendicular to the surface and is the vector sum of q_{yz} and q_{zy} for a circular contact, that is:

$$|q_{orth}| = \left(q_{yz}^2 + q_{zx}^2\right) = 0.21P_o \quad \text{(Eq 2)}$$

where x and y are the two axes of the contact circle. For elliptical contacts, x any y indicate the major and minor axes of the contact ellipse. Although the magnitude of orthogonal shear stress is the same at the leading and trailing edge of the contact region for a dry, frictionless contact, the direction is reversed to give rise to maximum $q_{orth(max)}$ and minimum $q_{orth(min)}$ values of orthogonal shear stress (Fig. 8). Hence, the maximum amplitude of orthogonal shear stress reversal, Δq_{orth}, is given as:

$$\Delta q_{orth} = (q_{orth(max)} - q_{orth(min)}) = 0.42P_o \quad \text{(Eq 3)}$$

Values relative to P_o indicated in Eq 1–3 will be different for elliptical contacts. Also, the location and magnitude of these stresses strongly depend on the value of the friction coefficient within the contact region. As the friction coefficient increases, the tangential loading shifts the location of maximum shear stress toward the surface. Similarly, the lubrication regime, surface roughness, and residual stress all affect the stress fields. Engineering Science Data Units (Ref 31, 32) tabulate the variation in these stress fields with friction coefficient and contact ellipse ratio.

Both maximum and orthogonal shear stress theories have been proposed to act as the subsurface failure modes during RCF. Fatigue life prediction theories, for example, the Lundberg-Palmgren theory (Ref 33), is also associated with the location of orthogonal shear stress. More recently, equivalent or effective shear stress (q_e) based upon the von Mises criteria (Ref 32–34) has been shown to support experimental investigations, that is:

$$q_e = \left[q_{xy}^2 + q_{yz}^2 + q_{zx}^2 + \tfrac{1}{6}\left\{\left(\sigma_x - \sigma_y\right)^2 + \left(\sigma_z - \sigma_x\right)^2 + \left(\sigma_z - \sigma_x\right)^2\right\}\right]^{1/2} \quad \text{(Eq 4)}$$

where σ_x, σ_y, and σ_z are the direct stress, and q_{xy}, q_{yz}, and q_{zx} are the shear stress values, respectively. This failure criterion for homogenous, isotropic, and ductile materials can be related to the critical value of effective shear stress ($q_{e(crit)}$) using the relation:

$$q_{e(crit)} = \sigma_{yield}^2 / 3 = \tau_y^2 \quad \text{(Eq 5)}$$

where σ_{yield} is the yield strength of material in uniaxial tension or compression, and τ_y is the yield stress in simple shear (Ref 32). Apart from the subsurface shear stress and von Mises criteria mentioned previously, maximum tensile (T_{max}) stress criteria is a useful indicator for appreciating RCF failure mechanism in brittle materials. It is postulated that cracks initiate and propagate from the tensile stress at the edge of the contact region (Fig. 8). The magnitude of T_{max} increases with the increase in friction coefficient; however,

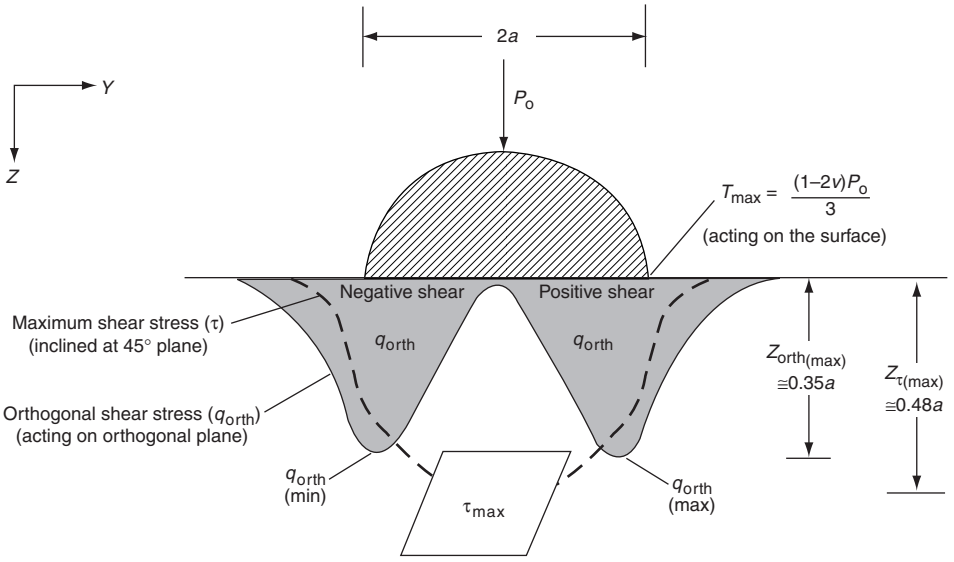

Fig. 8 Two-dimensional schematic of variation in critical stress components with depth for a circular rolling contact of diameter 2*a*

Table 1 Summary of RCF testing methods

Method	Description	Ref
NASA five-ball testing apparatus	Four lower balls, freely rotation 90° apart in a separator; simulates the kinematics of a thrust-loaded bearing; the contact angle can be varied; vibration sensor detects failure in unattended tests; low- (cryo) and high-temperature testing (to 1000 °C, or 1830 °F)	26 (a)
Flat-washer testing apparatus	16 retained balls rolling in a circle on a flat washer with a 75 mm (3 in.) outside diameter, 50 mm (2 in.) bore, and 6.4 mm (¼ in.) thickness; 4.17 GPa (605 ksi) contact stress; 1500 rpm; filtered lubricant delivery system; piezo sensor detects vibration	26 (b)
Unisteel testing apparatus	Flat washer on retained balls; hanging dead-weight load; contact stress approximately 4.5 GPa (650 ksi); 1500 rpm; drip feed of lubricant; vibration detection system; thermocouples monitor temperature (typically 50 to 60 °C, or 120 to 140 °F)	26 (c)
Rolling-contact testing apparatus	Two hemispherically ground, toroidal rollers loaded against a round bar; 40:1 ratio of roller diameter to bar diameter; 2.7 to 5.5 GPa (390 to 800 ksi) contact stress; 12,500 rpm; drip-feed lubrication; velocity-vibration sensor	26 (d)
Ball-rod testing apparatus (Federal-Mogul)	Three 12.5 mm (½ in.) balls loaded against a rotating 9.5 mm (⅜ in.) outside diameter center rod; 3600 rpm; spring load on opposing tapered retaining rings; accelerometer coupled with a shutdown device; drip-feed lubrication; stress per ball typically 6 GPa (870 ksi)	26 (e)
Cylinder-to-ball testing apparatus	Symmetrical arrangement of two 19 mm (¾ in.) balls rolling on a 12.5 mm (½ in.) outside diameter captive cylinder; coiled-spring load through a multiplying lever; small cylinder rpm = 22,677; splash lubrication; maximum contact stress, 5.8 GPa (840 ksi)	26 (f)
Cylinder-to-cylinder testing apparatus	Symmetrical arrangement of two 12.5 mm (½ in.) cylinders on two 20 mm (0.8 in.) outside diameter captive cylinders; coiled-spring load through a multiplying lever; small cylinder, cpm = 20,400; splash lubrication; maximum contact stress less than 4.4 GPa (640 ksi); vibration sensor terminates test	26 (g)
Ring-on-ring testing apparatus	Crowned rings rolling on their peripheries; ring diameters of 50 and 53 mm (2 and 2.1 in.) provide "no-slip" condition, but various degrees of slip are possible by changing ring diameters; typically 2000 rpm; contact ratio measured by electrical resistance; contact stress range typically 0.98 to 3.9 GPa (140 to 570 ksi)	26 (h)
Various types	Method of testing for rolling contact fatigue of bearing steels	26 (i)
Multiple bearing testing apparatus	Deep-groove ball bearing design; typically 3000 rpm; four bearings on a single center shaft; maximum contact stress, 2.9 GPa (420 ksi); accelerometers on the outer housing monitor failure	26 (j)
Rolling four-ball testing apparatus	Top ball drives three lower balls in a tetragonal arrangement; lower balls free to rotate in the cup; all balls 12.5 (½ in.) diam; upper balls spindle speed, 1500 rpm; 5.9 kN (1325 lbf) load applied vertically	26 (k)
High-speed four-ball testing apparatus	Same arrangement as above, but speeds of 15,000 to 20,000 rpm; operating temperatures often exceed 100 °C (210 °F) (Plint machine)	26 (k)
"AOL" vertical testing apparatus	11 retained balls clamped between two flat washers; thrust load; recirculating lubricant system	26 (k)
Inclined ball-on-disk testing apparatus	Spindle-held 20.5 mm (0.8 in.) ball rolling on a disk; up to 800 °C (1470 °F); ball speed up to 7200 rpm; disk speed up to 3600 rpm; variable slide/roll ratios; traction measurements; designed for ceramics	27

Further information can be found on the following pages of Ref 26: (a) p 5–45, (b) p 46–66, (c) p 67–84, (d) p 85–106, (e) p 107–124, (f) p 125–135, (g) p 136–149, (h) p 150–165, (i) p 169–189, (j) p 206–218, (k) p 219–236. Source Ref 13.

Note: NASA, National Aeronautics and Space Administration

its location remains very near the surface. For a frictionless, dry contact, the value of T_{max} can be approximated using the relation:

$$T_{max} = (1 - 2\nu)P_o/3 \quad \text{(Eq 6)}$$

where ν is the Poisson's ratio.

Rolling Bearing Life. Life prediction of a roller or ball bearing is based on the statistical treatment of full-scale bearing tests conducted under controlled environments, for example, full-film lubrication regime, dust-free environment, and so on. Although these controlled environments are useful indicators of the RCF performance of rolling-element bearings, the actual life of a given bearing can significantly vary from the predicted life. It was reported that only 10% of all bearing replacements in the field can be attributed to classic RCF failure (Ref 35), whereas the remaining 90% are made for reasons and conditions not even closely related to RCF (Ref 26). Although this highlights the improvements achieved in designing and manufacturing better-quality bearings, it also indicates that other factors in addition to RCF need to be considered to predict the life of a bearing. Even under the controlled conditions of load, lubrication, and alignment in a dust-, corrosion-, and moisture-free environment, there is generally a large scatter in the RCF performance for a given bearing. Bearing manufacturers thus provide a statistical probability of the life of a bearing on the basis of experimental results conducted at a given load, speed, and lubrication regime. Weibull analysis (Ref 17) can then be used to estimate the life expectancy of the bearing. Bearing life is generally referred to as L_{10}, L_{50} or L_{90} and indicate the probability of failure (e.g., L_{10} indicates that 10% of the bearings in a given population will fail before a fixed number of stress cycles are reached). Lundberg and Palmgren developed a theory that indicates the life of a roller or ball bearing at a given load (P) can be approximated using the relation:

$$L = (C/P)^n \quad \text{(Eq 7)}$$

where L is the fatigue life in a million revolutions, C is the load that gives an L_{10} life of 1 million revolutions, and n is a constant for a bearing type (e.g., $n = 3$ for ball bearings and 10/3 for roller bearings). A detailed list of various values of n for different bearing types can be seen elsewhere (Ref 36). The use of a specific value of n is critical for a given bearing type, and the product law of probability is in effect (e.g., as the design changes from single-row to double-row bearings). Hence, the life of a double-row bearing under similar conditions to that of a single-row bearing of identical design will be less than that of a single-row bearing. A detailed account of the statistical treatment of life predictions for a variety of bearing types can be found in Ref 36, which also indicates the importance of lubrication regime for such analysis. In addition to lubrication regime, material shakedown effects (e.g., Ref 37, 38) and the role of residual stress (e.g., Ref 39–42) on the RCF life can be significant. Apart from Weibull analysis and the Lundberg-Palmgren theory, other theories of fatigue-life prediction (Ref 18) can also be used. These theories were compared recently using a model roller-race contact and the study indicated that the accuracy of individual theories depends not only on the life equation used but also on the assumed Weibull slope (Ref 8). The final choice of these parameters should therefore be consistent with the experimental investigations.

Rolling-Contact Fatigue of Vapor-Deposited Coatings

Advancements in rolling-bearing technology, such as the introduction of hybrid ceramic bearings that use the superior mechanical and thermal properties of ceramic balls, indicated that their full potential could only be realized by improving the performance of bearing races. Conventional materials and manufacturing processes for the fabrication of steel races were, however, at the limit of established technology, and there was a technological gap demanding an innovative approach to further improve rolling-bearing life in hostile environments. Overlay coatings such as those deposited by the physical vapor deposition (PVD) processes, which had already shown remarkable improvements in the cutting-tool technology, provided this innovation and improved the fatigue resistance of coated steel races to match that of ceramic balls. This combination of coated races and ceramic balls resulted in rolling bearings of improved performance, for example, higher rotational speeds in roller bearings for machine tool spindles (Ref 43) and pump bearings for the space shuttle main engines (Ref 44). In addition to steel races, the uses of PVD coatings have now been commercially extended to coated rollers and also coated rolling-element balls, thereby extending the performance of conventional steel bearings. The versatility of materials available for PVD coating processes provides an exotic combination of single- and multilayer functionally graded materials, for example, TiN, CrN, diamond-like carbon (DLC), and anti-friction layers of solid lubricants for space technology, for example, MoS_2 coatings. The scope of this article is, however, limited to the RCF performance of hard overlay coatings in general, with specific details of underpinning failure mechanisms of TiN and DLC coatings.

Physical vapor deposition is a gaseous-state process in which coating material is atomized or vaporized to deposit a coating. The success of PVD coatings in rolling-bearing technology (Ref 43–60) owes its existence to the advancements in PVD coating processes and, in particular, their ability to deposit these overlay coatings at a lower temperature, that is, with minimum residual stress in the coating layer(s) to avoid premature delamination. The commercialization of competing overlay coating technologies for RCF applications, for example, chemical vapor deposition (CVD) and thermal spraying (TS), is in its infancy in comparison to PVD. However, despite the enormous success of PVD coatings, these competing technologies offer additional technological and economical incentives. For example, the coating thickness of CVD and TS coatings can be orders of magnitude greater than that of PVD deposits (which is seldom over 5 μm). Rolling-contact fatigue properties of substrate become less important as the coating thickness increases beyond the depth of maximum shear stress, providing the ability to combat both surface- and subsurface-initiated RCF. In addition, the high deposition rates and low cost of TS in comparison to PVD/CVD coatings provide economical incentives. Because the nature of the TS process and the resulting coating microstructure are very different from that of PVD/CVD coatings, the investigations of TS coatings for RCF applications are covered in a separate section of this article. This section deals with the RCF investigations of PVD/CVD coatings. For the description of various PVD, CVD, and TS coating processes considered in this article, readers are referred to Ref 48 and 49.

Despite the enormous success of overlay coatings in improving the RCF performance of rolling bearings, theories relating to the life prediction of coated rolling bearings are in their infancy. Most recently, research attempts in this field were made for particular bearing types, for example, NU1008 (Ref 44–46). The researchers concluded that RCF life of TiAlN coatings, in general, is consistent with the loading recommendations of bearing catalogs. Such investigations are crucial for generic solutions leading to RCF life prediction in coated components. Future studies in this area to include the effects of surface roughness, lubrication regime, and residual stress (Ref 61) are therefore inevitable before such models can be generally applied to estimate the RCF performance of coated rolling bearings. In one such attempt to include surface roughness effects (Ref 47), it was concluded that significant improvements in the RCF life of coated bearings can be made by applying relatively thicker (coating thickness $\geq$ 3 μm), well-adhered coatings with fine microstructure to avoid cohesive failure in thick coatings. However, due to the inherent complexity of interaction of various tribological factors that influence the RCF life prediction of coated surfaces, most of the investigations in this field are based on experimental evaluations under accelerated RCF test conditions using various RCF tribometers referred to in Table 1.

Rolling-Contact Fatigue Performance of PVD Coatings. Table 2 catalogs the results of various RCF investigations of PVD coatings (Ref 43, 50–60). It can be appreciated from Table 2 that even at relatively high contact stress levels (in excess of 4.0 GPa, or $0.6 \times 10_6$ psi), the RCF performance of PVD coatings can be well over several hundred-million cycles without failure. These investigations indicate that the RCF performance of nitride (especially TiN and HfN)

and DLC coatings can easily outperform conventional bearing materials, whereas other coating materials such as CrN show a promise for the future. Sputtering (either reactive, ionic, or magnetron) and ionic beam deposition have been the preferred PVD coating process for nitride and DLC coatings, respectively.

Although PVD coating deposition parameters used to deposit the coatings for these RCF investigations have not been indicated in Table 2, they can have significant influence on coating microstructure and thus its RCF performance; for example, for reactive sputtering of TiN coatings, intercolumnar porosity of TiN coatings can be decreased by increasing the substrate temperature (Ref 62). However, the influence of PVD deposition conditions (parameters) on the RCF performance has not yet been clearly addressed in published literature. For now, it can be assumed that the coatings referred to in Table 2 were deposited under the best-known deposition conditions available for specific coating material and PVD process. Wherever possible, the RCF performance levels in Table 2 are quoted in terms of L_{10}, L_{50}, or average life for statistical comparison. However, these results are generally qualitative and should be used as the basis of rating the RCF performance of various coatings rather than to predict the statistical RCF life.

Table 2 also indicates that the RCF results are sensitive to parameters such as coating thickness, substrate hardness, and lubrication regime. Even for the best possible combination of coating thickness, substrate hardness, and lubrication (e.g., in TiN coatings of less than 1 μm coating thickness), potential RCF improvements have been shown to vary, depending on the surface roughness of the contacting pair (Ref 51). Such investigations indicate that for very smooth surfaces of rolling-contact bodies, the improvements in RCF performance by the application of PVD coatings can be marginal. However, rolling bearings generally operate under harsh tribological environments, and potential RCF improvements by surface coatings are generally realized in most industrial applications. Table 2 also indicates the significant scatter in RCF performance while comparing the results from various accelerated RCF test methods. Even for a given test method and coating, variations in stress levels have shown significant variations in potential

Table 2 Published findings for RCF performance of PVD coatings

Coating process	Coating material	Substrate	RCF tester	Contact stress, GPa	Coating thickness, μm	Coating roughness R_a, μm	Coating hardness	Substrate hardness	RCF life, $\times 10^6$ cycles	Ref (year)
Ionic sputtering	CrN Mo TiAlN TiAlCN TiCN TiN + C	100Cr6	Ball on rod, full scale bearing tests (lubricated)	Contact load of 755 N for ball on rod	2.5 2.5 2.0 2.0 2.0 1.0	N/A	1300 650 2900 1800 2200 900	N/A	<100 (average) <100 (average) >250 (average) >250 (average) >250 (average) >1000 (average)	43 (1996)
Ion plating	TiN	Tool steel	Ball on cylinder	3.5, 4.6, 5.1	2 → 5	0.03 ± 0.01 0.15 ± 0.01	50 → 60 HRC	2300 HV	<1.3 (average)	50 (1998)
Reactive sputtering	TiN	M50 bearing steel	Three-ball on rod (lubricated)	5.5	0.25, 0.5, 0.75, 1, 2, 3, 5	0.05 → 0.1	30 GPa	59–60 HRC	>100 (for coating thickness <1 μm)(a)	51 (1998)
Ion plating, magnetron sputtering	TiN Ti(CN) CrN	High speed steel	Amsler wear tester (dry)	50 N (load)	1.8–3.5 1.8–3.4 3.5	0.9 ± 0.1	N/A	N/A	1 1 5	52 (1998)
Reactive magnetron sputtering	TiN ZrN HfN CrN Mo TiAlN TiZrN (TiAlV)N	440C stainless steel (RCF life of 6.3 and 1.7×10^6 cycles at 4.0 and 5.4 GPa)	Three-ball on rod (lubricated)	4.0 and 5.4	0.25, 0.5, 0.75, 1.00	N/A	55 → 59 HRC	59 HRC	36 and 8.7 (L_{10})(b) 36 and 5.5 (L_{10})(b) 81 and 9.7 (L_{10})(b) 21.6 and 2.0 (L_{10})(b) 39.9 and 5.0 (L_{10})(b) 2.6 and 1.6 (L_{10})(b) 21.5 and 10.8 (L_{10})(b) 47.9 and 10.3 (L_{10})(b)	53 (1993)
Reactive sputtering	TiN	AISI 4118 steel	Two-disc (lubricated)	2.3	0.25–0.5 1.0 2.5 5.0	N/A	N/A	N/A	>60 10–37 1.0–4.1 <0.1	54 (1990)
Reactive sputtering	TiN	AISI 4118 steel	Two-disc (lubricated) roll/slip ≈ 0.25	2.3	1.0	0.45	2300 kgf/mm^2	62–64 HRC	>33 (average)	55 (1991)
Reactive sputtering	TiN TiAlN CrN	Si_3N_4 and M50	Four-ball (lubricated)	5.8 and 6.8	0.3–1.0	N/A	N/A	N/A	<100 for 0.75 μm TiN at 5.84 GPa(c)	56 (1994)
Magnetron sputtering	TiN/NbN	M50	Three-ball on rod (lubricated)	3.4 5.2	0.5	0.075–0.1	5200 kgf/mm^2	561–63 HRC	191(d) 15(d) (L_{10} in hours)	57 (1998)
Ion beam	DLHC	M50 AISI 52100 AISI 4118 AISI 440C	Three-ball on rod (lubricated)	5.5	0.5 → 1	0.06 → 0.07	N/A	N/A	76.4 (L_{50} life), 10(e) 232 (L_{50} life), 14(e) 327 (L_{50} life), 10(e) 22.7 (L_{50} life), 3.7(e)	58 (1993)
Ion beam	DLC	M50	Three ball on rod (lubricated)	5.5	0.5 → 1	N/A	11.3 → 14.7 GPa at 25 g load	10.8 GPa at 25 g load	1 to 300(f)	59 (1992)
Ion beam	DLC	M50	Three ball on rod (lubricated)	4.8	0.33	N/A	N/A	N/A	91.5 at 23 °C (73 °F) (L_{50})(g) 45.9 at 177 °C (73 °F) (L_{50})(g)	60 (1997)

Note: AISI, American Iron and Steel Institute; DLHC, diamond-like hydro-carbon. (a) Best performance at L_{50} of 25×10^6 and $>100 \times 10^6$ with rough and smooth balls, respectively, for coating thickness <1 μm. (b) Best L_{10} values quoted, which relate to coating thickness range of 0.5–0.75 μm at two stress levels of 4.0 and 5.4 GPa, respectively. (c) All coatings in hybrid ceramic combinations showed improvement in average RCF life, with best average improvement by a factor of 2.5 for 0.75 μm TiN coating over uncoated case. (d) L_{10} values quoted in hours for superlattice period of 3–6 nm at respective stress level. Uncoated M50 substrate had L_{10} of 39 and 9 h at stress levels of 3.4 and 5.2 GPa, respectively. (e) L_{50} improvement factor over uncoated case. (f) L_{50} and L_{10} of 13×10^6 and 0.6×10^6, respectively, with no significant influence of coating thickness. (g) L_{10} of 36.7×10^6 and 38.4×10^6 at 23 and 177 °C (73 and 351 °F), respectively.

RCF improvements. Nevertheless, the performance indicators referred to in Table 2 have also been shown to match that of full-scale bearing tests (Ref 63). It is worth appreciating that this dependency of RCF performance on various tribological design parameters and RCF test methods is not unique to overlay coatings. Conventional steel bearings often display such dependency, with the exception that this interdependency in the case of surface coatings is much more complex due to additional influential factors such as coating microstructure, thickness, and interfacial bond strength.

The dependence of RCF performance on the tribological design parameters, such as coating thickness, substrate hardness, tribological condition of contact stress, lubrication regime, and surface topography, can actually be understood by a generic understanding of underlying failure modes. What dictates the influence of the previously mentioned design factors is their sensitivity to initiate and propagate various RCF failure modes, the understanding of which cannot only provide better life prediction models but also improved RCF performance of coated rolling bearings. As indicated earlier, the lack of data on all coating materials has made it almost impossible to ascertain their failure modes, although their RCF performance is represented in Table 2. The scope of the remaining section is hence focused to ascertain the underlying failure mechanisms of the two most widely used PVD coating materials, that is, TiN and DLC coatings. Before embarking on the discussion of the failure mechanism of these coating materials, it is important to appreciate the generics of the tribological design approach adapted to improve RCF performance by the application of PVD coatings.

Tribological Concept of Depositing Thin Coatings to Improve RCF Performance. Physical vapor deposition coatings, which are strongly adhered to the substrate, are very thin and seldom over a few microns in thickness. These thin coatings generally follow the topography of the substrate material, so that there is no appreciable improvement in the surface roughness of the coated substrate. So, how does such a thin coating improve the RCF performance? Figures 2 and 8 indicated various crack initiation sites during a contact loading. Obviously, such a thin coating in contact with a smooth counterbody marginally affects the depth of orthogonal, maximum shear or von Mises stress. Also, the influence of a thin coating on the subsurface stress distribution is marginal for low values of coating-to-substrate modulus ratio (Ref 64, 65). Hence, these thin coatings do not improve the resistance to subsurface fatigue crack initiation and propagation. However, the near-surface stress field and near-surface crack initiation and propagation can be seriously affected by the application of such hard coatings. This is achieved by the interaction of the hard coating layer on the counterbody, which initiates its micropolishing either in two-body abrasion (e.g., for TiN coatings) or in three-body abrasion (e.g., for DLC coatings) to improve the overall RCF performance of the contacting pair by minimizing the stress protrusions at individual asperity contact. In essence, these coatings tend to delay near-surface crack initiation, which is thought to constitute 90% of the total life to RCF failure (Ref 60). In addition, improvement in frictional properties of the contacting pair, for example, by DLC and molybdenum coatings, provides additional improvements in RCF performance.

Rolling-Contact Fatigue Failure Modes of PVD Coatings. Despite numerous studies to comprehend the RCF performance of PVD coatings (Table 2), only a few have attempted to outline a fundamental understanding of failure mechanisms. Some studies (Ref 51, 53–55, 58–60) only begin to understand the underpinning failure mechanisms of PVD coatings, as discussed subsequently for TiN and DLC coatings.

Failure Modes of PVD-TiN Coatings. The structure of TiN coating deposited by various PVD processes is generally columnar with some evidence of equiaxial grains near the interface (Ref 50, 51). These coatings have shown good bonding with various substrate steels, for example, M50, 440C, and so on, and also, TiN coatings on Si_3N_4 ceramics (Ref 56) have been successfully applied. Apart from good bonding of TiN coating either directly onto the substrate or by functional grading, the most important substrate property, which dictates the RCF performance of coated rolling elements, is substrate hardness. The choice of substrate material and coating deposition conditions are therefore critical to allow the retention of substrate hardness after deposition. Failure to retain substrate hardness after deposition adversely affects the RCF performance (Ref 50, 53). The underlying failure mechanism caused by a reduction in substrate hardness is principally due not only to a compromise in the ability of substrate to support the coating, but also to microstructural changes associated with substrate softening that can result in stress concentrations and create fatigue initiation sites. Hence, tribological design of these coatings must not only aim for a well-bonded coating but also for the retention of substrate hardness.

In addition to substrate bonding and its hardness, the most critical parameter that has been shown to significantly influence the RCF performance of TiN coatings is coating thickness. TiN-coated cutting tools are generally coated up to a coating thickness of 3 μm. However, investigations have shown that such coating thickness can adversely affect the RCF performance. In fact, the optimal thickness for improved performance is generally reported as approximately 0.5–0.75 μm (Ref 51, 53, 54, 56). So, why does any increase in coating thickness beyond this level adversely affect the RCF performance? The answer to this question lies in the TiN coating microstructure, and there are two schools of thought that explain this dramatic influence of coating thickness: adhesive failure of thicker coatings (Ref 50, 52, 54, 55) and cohesive failure (Ref 51).

Polonsky et al. (Ref 51) argued that even in a good-quality PVD (TiN) coating with negligible porosity, the columnar coating microstructure becomes coarser away from the interface. Hence, an increase in coating thickness causes competitive growth during film deposition. (Although it was assumed that the best available deposition conditions were used to deposit the PVD coatings listed in Table 2, it is worth appreciating that these are not entirely defect-free coatings, and further improvements in RCF performance of PVD coatings can be realized by improved coating microstructure.) The interfaces between these columns thus represent the crack initiation sites within the coating microstructure, the probability of which (i.e., defects at column boundaries) increases with the coating thickness. Hence, the coating fails cohesively with the increase in coating thickness—and the failed coating area is very rough due to shear within the columnar coating microstructure—rather than adhesively at the interface. Contrary to this, some studies (Ref 50, 52, 54, 55) suggest that the weakest section in the coated rolling element is the coating-substrate interface, and hence, the failure is adhesive. The substrate hardness can further influence the failure mechanism in TiN coatings, (Ref 50) as shown in Fig. 9—that is, cracks propagate perpendicular to the coating substrate interface for softer substrate coatings (Fig. 9a), and parallel to the coating-substrate interface for harder substrates (Fig. 9b, c). From Fig. 9, it is striking to note that for the scanning electron microscope representation of failed areas for harder substrates (Fig. 9b, c), which are more closely related to the tribological conditions reported in Ref 50, the failure is just above the coating-substrate interface (i.e., similar to a cohesive failure) rather than at the coating-substrate interface. Hence, there seems to be consistent experimental evidence pointing to cohesive, rather than adhesive failure of thicker TiN coatings. The theory of adhesive failure presented in Ref 50, 52, 54, and 55 thus relies on weakness of the coating-substrate interface to explain the influence of increase in coating thickness on reduced RCF performance. Reference 50 also suggests the theory put forward in Ref 66, which relates the cyclic shear stress to crack initiation; this seems unlikely, because the depth of maximum and orthogonal shear stress for the smooth, lubricated contacts considered in the experimental study can be an order of magnitude deeper than the coating thickness.

Another reason for the adhesive failure of thicker coatings can be understood by comparing the Young's modulus of the coating to that of the substrate material. It is postulated that as the difference in Young's modulus increases, thicker coatings resist to follow the elastically deformed profile of the substrate (under the contact region in response to cyclic loading), whereas thinner coatings tend to follow a similar profile as the elastically deformed substrate. This could lead to premature failure in thicker TiN coatings. More recently, however, work reported on TiAlN coatings (Ref 44) has indicated that as the dif-

ference in the modulus between the coating and substrate material increases, even for smooth contact surfaces, the coating-substrate interface can be subjected to a high degree of shear stress in thin (2–3 μm thick) PVD coatings. Similar results were reported in Ref 64. Functional grading of the coating can thus be useful to improve the RCF performance of thicker coatings.

Even if some of the reported failures (Ref 50, 52, 54, 55) were considered truly adhesive, the test methodologies in these studies were very much alike (i.e., two-disc machine or its modification) and very different to the ball-on-rod test method (Ref 51), which shows cohesive failure. Hence, the model contact geometry can be responsible for the change in failure mode, which is also known to influence the failure mode in conventional ceramics and steels (Ref 67). Also, there were considerable differences in substrate shakedown behavior. Some studies (Ref 51) indicated substrate yielding in the first few cycles, due to high contact stress that was above the yield strength of the substrate M50 steel. This shakedown effect (Ref 37, 38) cannot only improve the RCF performance by substrate work hardening and improved coating-substrate conformity near their interface, but also influence the RCF failure mode. Contrary to this, studies reported in Ref 50, 52, 54, and 55 did not indicate any such shakedown effects. Hence, the difference between the two test conditions can also be thought responsible for the reported differences in cohesive and adhesive failures.

The tribological explanation of how thinner (0.25–0.75 μm) PVD coatings avoid cohesive and adhesive failure and thus improve the RCF life lies in the microcontacts within the Hertzian contact area. Thinner TiN coatings, which do not fail during the RCF tests, do not show any change in their surface roughness, apart from surface glazing. The surface of the counterbody, generally steel, however, undergoes micropolishing during the RCF test. This micropolishing reduces the stress protrusions at the asperity level, which is generally thought to be responsible for near-surface initiation of RCF failure. Indeed, it has been confirmed that for very smooth counterbodies—for example, grade 24 steel balls in their study (R_a = 0.01 μm)—the contacting surfaces did not have any further scope of micropolishing, and hence, no substantial increase in RCF performance was obtained (Ref 51). However, it is worth appreciating that it is not only the surface roughness but also the hardness difference of the contacting pair and their friction properties, that also dictate the RCF performance of coated rolling-element bearings. Rolling bearings generally operate in harsh tribological environments, and the scope of improvement in RCF performance by coating application is always realized, for example for self-mated TiN couples in pure rolling or rolling/sliding contacts (Ref 52), and by Igartua et al. (Ref 43) for hybrid ceramic bearings where the counterbody is a ceramic of similar hardness to a TiN coating.

The theory of interaction of surface asperities to provide micropolishing and subsequent improvements in RCF life also provides some clues as to why nitride coatings (Ref 53), thinner than 0.25 μm provide only marginal RCF improvements. According to the aforementioned theories of cohesive and adhesive failure in TiN coatings, a thinner coating should theoretically provide a better resistance to both failure mechanisms, that is, thinner coatings have less probability of intercolumnar coarsening and hence low probability of cohesive failure. Also, thinner coatings should adequately follow the deformed substrate profile, so low stress concentrations at the interface should resist adhesive failure. Marginal RCF improvements for coatings thinner than 0.25 μm can, however, be explained in terms of the influence of the substrate surface roughness. Even for a smooth substrate, the peak-to-valley height of the surface profile can be significantly greater than the average (R_a) surface roughness. A thinner coating may, therefore, only provide partial protection to surface asperities, especially in the valleys of the surface profile, for example, due to shadowing effects. This can minimize the rate of micropolishing of the counterbody, and hence, the delay in crack initiation is not maximized, which is essential for optimizing the RCF performance.

Failure Modes of PVD-Diamond-Like Hydrocarbon (DLHC)/DLC Coatings. Superior tribological properties of DLC coatings (Ref 48) have

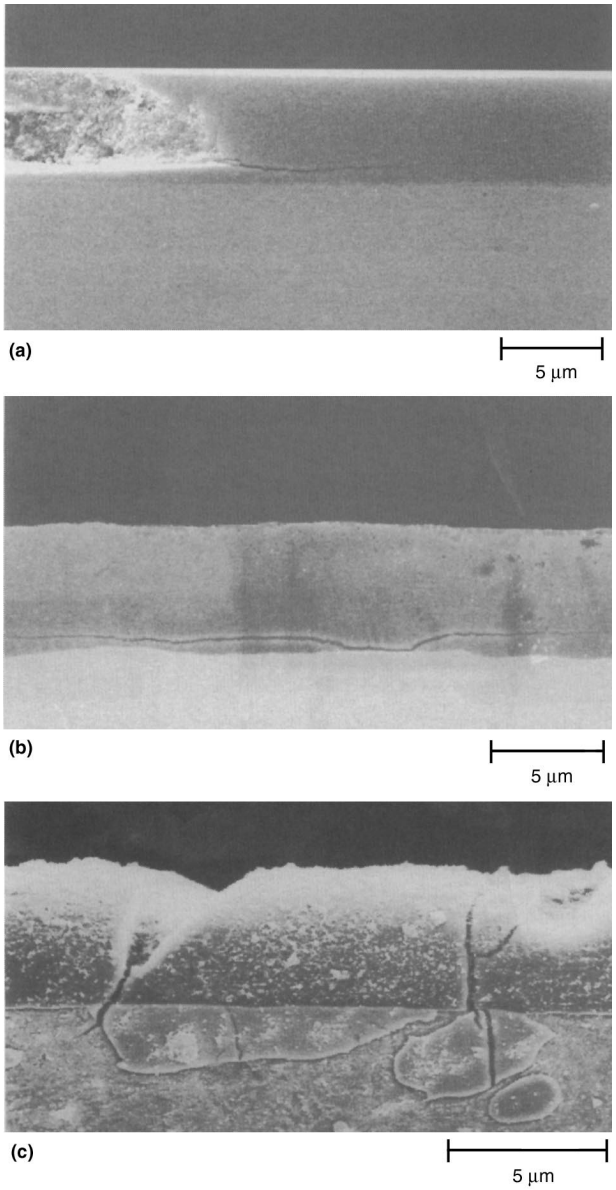

Fig. 9 Morphology of cracks leading to rolling-contact fatigue failure of PVD (TiN) coatings. (a) Crack parallel to the interface leading to spalled area for hard substrate (60 HRC) TiN coating. (b) Cracks parallel to the coating-substrate interface for hard substrate (60 HRC) TiN coating. (c) Cracks perpendicular to the coating-substrate interface for soft substrate (50 HRC) TiN coating. Source: Ref 50

shown considerable promise in improving the RCF life of coated rolling elements. References 58 and 59 and, more recently Ref 60, reported most of the work in this field. As with the TiN coatings, these results relate to investigations in mixed lubrication regimes. Except for the room-temperature RCF studies reported in Ref 60 (Table 2), where coatings were much thinner (~33 nm) than those considered in Ref 58 and 59 (0.5–1 μm), both DLC and DLHC coatings have been shown to provide considerable improvements in the RCF life of coated rolling elements. The physical mechanism underpinning such improvement is although different from that of TiN coatings (mentioned previously); however, the underlying analogy to micropolishing is the same.

In the studies reported in Ref 58 and 59, two tribological mechanisms are thought to be responsible for the improvement of RCF life. The first mechanism is three-body abrasion, leading to the micropolishing of the counterbody and thus lowering stress protrusions within the contact region at the asperity level. This three-body abrasion is thought to be caused by the delaminated DLC or DLHC coating particles during RCF testing, which, when mixed with test lubricant, polish the softer surface within the contact region. Wei et al. (Ref 58, 59) postulated that this mechanism was due to the absence of diamond film at the time of spall or at the end of the terminated tests. This essentially refers to the same mechanism of micropolishing as was reported for TiN coatings, except for the fact that the micropolishing is in three-body abrasion. The second mechanism thought responsible for improved RCF performance is the gradual graphitization of the DLHC film during the RCF test, leading to reduced friction at asperity level, and hence a delay in the surface-initiated RCF. This also explains the less dramatic influence of the DLC/DLHC coating thickness in the range 0.5–1.0 μm, and further supports the theory that coating detachment is responsible for RCF improvement, namely, three-body abrasion. Although for much thinner coatings (~33 nm), in which there was no RCF improvement seen at room-temperature tests (Ref 60), it is worth appreciating that there was no evidence of delamination, which is thought to be essential for micropolishing of asperities and hence, RCF improvement. Tests conducted at a higher temperature (175 °C, or 350 °F) with these thinner (~33 nm) coatings, however, showed some improvement to the RCF life. The exact mechanism leading to this improvement is not clear at this stage.

Rolling-Contact Fatigue of CVD Coatings. By using smoother contact bodies to suppress the mechanism of micropolishing within the coating region (Ref 51), very thin coatings could not provide significant improvement in RCF performance. In such cases, coating needs to be relatively thick (coating thickness ≥3 μm) and should have very high cohesive strength to provide RCF improvements. Chemical vapor deposition coatings, which have the versatility to deposit much thicker layers, can thus provide useful improvements in RCF life. Coatings in the thickness range of 3–190 μm have therefore been the focus of some RCF studies. However, the establishment of tribological data that could lead to generic design and understanding of failure modes in CVD coatings is in its infancy. Rolling-contact fatigue performance data of specific coating types is, however, available, as listed in Table 3 (Ref 68–73). Among these coatings, titanium-base nitride coatings have shown RCF performance up to a maximum of 50 million stress cycles. This does not match the extraordinary performance indicated earlier for PVD coatings; nevertheless, it is worth appreciating that some of these investigations (Ref 68, 69) were carried out to measure the bond strength rather than the RCF performance of these coatings, and tests were suspended after a specific number of stress cycles. The best performance for CVD coatings was reported in Ref 73 for TiC coatings. They showed that for CVD-coated TiC rolling-element balls, bearings can last in excess of 900 million revolutions in full-scale testing, and also that CVD coatings delayed the onset of lubricant degradation by reducing the effect of cold welding within the microcontact region.

The real advantage of CVD coatings is, however, in their ability to deposit layers that are an order of magnitude thicker than PVD coatings. Chao et al. (Ref 72) have recently reported that not only the coating thickness but also the beneficial compressive stress tailored in these thicker CVD coatings can be used to combat RCF failure. Although the best performance achieved in their setup was in excess of 50 million stress cycles for a 190 μm thick SiC coating with 680 MPa (100 ksi) compressive residual stress, these tests were suspended due to the failure of the steel balls rather than the coating. For those coatings that failed, the failure was cohesive, and the authors argued that the failure was due to discontinuous growth of SiC film. Such discontinuous growth may, however, be combated by appropriate selection of deposition conditions. In general, limited studies indicate that CVD-coated bearings outperform conventional bearing steels (Ref 72, 73), and future studies are inevitable to comprehend the underpinning failure mechanisms of these coatings.

Rolling-Contact Fatigue of TS Coatings

Thermal spraying is a molten- or semimolten-state process in which coating material in the form of a wire, rod, or powder is heated by combustion, gas plasma, or electric arc and accelerated toward the substrate to deposit a coating. The most commonly used classification of TS processes is based on the method of heat generation, and the most commonly used processes considered for RCF investigations are high-velocity oxyfuel (HVOF), detonation-gun (D-gun), and plasma spraying (PS). Within each category of these processes, there are sub-classifications, for example, HVOF can be liquid fueled or gas fueled, and PS can be air plasma sprayed (APS) or vacuum plasma sprayed (VPS). For details of various TS processes, readers are referred to Ref 49.

The coating materials available for TS processes range from high-abrasion-resistant ceram-

Table 3 Published findings for RCF performance of CVD coatings

Coating process	Coating	Substrate	RCF tester	Contact stress, GPa	Coating thickness, μm	Surface roughness, μm	Coating hardness	Substrate hardness, HRC	Fatigue life, $\times 10^6$ cycles	Ref (year)
PACVD	TiN (TiSi)N	High-speed steel	N/A	Equivalent bond stress of 800 MPa	3 → 4	0.6	2000 → 2500 HV	63–65	5 (suspended tests)	68 (1995)
PCVD	TiN	High-speed steel	Spherical	0.8	2.7	0.04	N/A	63	>5	69 (1997)
	TiCN			1.7 (estimated)				45–63	>50 <0.1 at higher stress for both coatings	
PECVD	TiN	High speed steel	Cylindrical spherical	Critical stress of 0.2–0.7	N/A	0.04	N/A	65	50 (at lower stress level)	70 (1998)
CVD	CrC-TiC	M50 bearing steel	Ball on rod, disc	2.76 → 4.83	5.4	0.02	64 HRC	65	5–10 × 10^6 (L_{50} life)	71 (1985)
CVD	SiC	SiC-TiC graphite	Three ball on rod	5.5	192	0.08	N/A	N/A	>50	72 (1995)
CVD	TiC	440C	Full scale	40 N load	3	0.005	35,000 MPa	N/A	>900 × 10^6 at 1400 rpm	73 (1993)

Note: PACVD, plasma-assisted chemical vapor deposition; PCVD, plasma chemical vapor deposition; PECVD, plasma-enhanced chemical vapor deposition

ics (e.g., Al_2O_3) and cermets (e.g., WC-Co) to abradabale coatings (e.g., polymer-based coatings for aeroengine applications). The coating microstructure of TS coatings is lamellar, and their industrial applications are found in aerospace, biomedical, automotive, and manufacturing industries. The advancements in TS technology, for example, liquid-fuel HVOF systems and VPS, made it possible to attain TS coatings with negligible porosity and minimum powder degradation, thereby improving the fracture toughness of TS coatings. Despite recent innovations in TS technology and its ever-expanding market share, RCF investigations of these coatings are in their infancy (Ref 74–83). The aim of this section is to comprehend the RCF performance and failure modes of TS coatings, with a view to defining the tribological design considerations. The rationale behind the RCF applications of TS coatings lies in their competitive advantages, which include:

- Very high deposition rates (typically 0.0025 kg/s, or 20 lb/h, for HVOF coatings)
- Ability to deposit thick coatings (up to a few mm) to resist both surface- and subsurface-initiated RCF
- Ability to produce coatings on large components
- Ability to restore worn or undersized components, making them environmentally friendly
- Wide range of coating and substrate materials
- Low deposition cost

Rolling-Contact Fatigue Performance of TS Coatings. Table 4 summarizes the RCF performance results for various TS coatings (Ref 74–83). As with the RCF performance of vapor deposition coating processes (Tables 2 and 3), these results are qualitative and should be considered to rank the RCF performance rather than for statistical fatigue-life prediction. These results indicate that the most commonly used TS coating material for RCF investigations is WC-Co cermet and Al_2O_3 ceramic. Among these coating materials, the RCF performance of cermets is superior to that of ceramics. The RCF performance of these coatings is, however, not as high as that associated with PVD (Table 2) coatings at stress levels greater than 3 GPa (0.4×10^6 psi) in point-contact loading. At moderate-to-low stress levels (up to 3 GPa, or 0.4×10^6 psi), these coatings, however, exhibit a RCF life in excess of 70 million stress cycles without failure. The scatter in RCF performance data shown in Table 4 is due to the influence of variations in tribological conditions as well as design parameters such as coating thickness, substrate hardness, and complexities in the coating microstructure. These design parameters significantly influence the RCF failure modes, as discussed subsequently.

Rolling-Contact Fatigue Failure Modes in TS Cermet (WC-Co) and Ceramic (Al_2O_3) Coatings. Investigations relating to the RCF failure modes of TS coatings are reported in Ref 7, 74, 79, 84, and 85. These investigations have classified the fatigue failure modes on the basis of surface and subsurface observations in pre- and post-RCF conditions. Rolling-contact fatigue failure of TS coatings are generally categorized in four main modes and named as abrasion, delamination, bulk failure, and spalling (M1–M4), as indicated in Fig. 10. A summary of the underpinning failure mechanisms leading to these failure modes is given subsequently, details of which can be seen in the aforementioned references.

Abrasive Failure of Coated Rolling Elements. The combined effect of micropitting and surface wear on the wear track of components in rolling contact is collectively termed as abrasive failure in TS coatings. This failure mode is seen with both ceramic (Al_2O_3) and cermet (WC-Co) coatings and with all TS coating techniques. A typical example of this failure is shown in Fig. 11. Noncontacting three-dimensional interferometry of failed wear track indicates that the micropits leading to abrasive failure are, on average, 50 μm wide and a maximum of 5 μm deep. Abrasive failure mode in TS coatings is thus not significantly different to those associated with rolling contact wear rolling contact wear (RCW) in conventional steel bearings; for example, Blau (Ref 13) has considered RCW as nucleation sites for initiating RCF. Similar failure was characterized as "peeling" during a study of fatigue failure modes of conventional steel ball bearings (Ref 16), whereas in Ref 5, this type of failure was characterized as surface distress. In spite of the various terminologies used to distinguish similar failure in steel bearings, the underpinning failure mechanism is associated with asperity contact in the presence of microslip within the contact region. Gross sliding, though not necessary for this type of failure, is thought to promote micropitting.

Mechanism of Coating Abrasion in Rolling/Sliding Contacts. In the case of TS coatings, a similar mechanism of asperity contact in the presence of microslip and sliding is responsible for the micropitting and surface wear. During partial elastohydrodynamic lubrication (EHL) conditions, that is, when lubrication regime is in the mixed region ($1 < \lambda < 3$, where λ is nondimensional film thickness), surface asperities come into contact. Under these conditions, it was

Table 4 Published findings for RCF performance of thermally sprayed coatings

Coating process	Coating material	Substrate material	RCF tester	Contact stress, MPa	Coating thickness, μm	Coating roughness (R_a), μm	Average coating hardness	Substrate hardness	RCF life, $\times 10^6$ cycles	Ref (year)
APS, HVOF	WC-12%Co WC-17%Co WC-10%Co-4%Cr	DIN 17200 steel	Two-disc (dry)	420–600	100	0.12–0.51	758–1208 HV	32–37 HRC	>10(a)	74 (1997)
HVOF	WC-Cr-Ni	JIS G4105 steel	Two-disc (lubricated)	2400–3000	20–90	0.2	940	790 HV	>20 (average)(b)	75 (1995)
D-gun	WC-15%Co Al_2O_3	M50 steel	Four-ball (lubricated)	3000–3400	70	0.04	1200 1050	658 HV	0.16–0.6 <0.1	76 (1997)
D-gun	WC-15%Co	M50 steel	Four-ball (lubricated)	3400 5200	50	0.02	1200	600 HV	2.9 0.4	77 (1996)
APS	Ni-B-Si-Cr-Fe-C	Steel	Two-disc (lubricated)	822, 845, 960, 1086	200 450	0.24	N/A	60 HRC	<5.5 <3	78 (2000)
HVOF	WC-Cr-Ni	S45C steel	Two-disc (lubricated)	1400	40–90	0.1	920	308–670 HV	>20(c)	79 (2000)
HVOF, D-gun	WC-12%Co	Steel	Three-disc Two-disc	410	100	0.35	1050, 1150	710 HV	. . .	80 (1994)
HVOF	WC-12%Co	Mild steel	Four-ball (lubricated)	1700–1900	20 50 150	0.05	1318	218 HV	>70(d) 2–20 15–30	81 (1997)
HVOF	WC-12%Co	440C steel	Four-ball (lubricated)	2700–3100	50 150 250	0.06	1296	850	<1.5 >70(d) >70(d)	82 (2001)
APS	Al_2O_3-TiO_2 Cr_2O_3-SiO_2-TiO_2 Mo	A2017 aluminium alloy	Two-disc (lubricated)	1500	300–350	N/A	805, 1089, 491	N/A	<10(e)	83 (1990)

(a) Best performance for HVOF WC-Co coating. (b) For coatings thicker than 40 μm. (c) For positive (≈12%) and zero slip ratio. (d) Test suspended after 70×10^6 stress cycles without failure. (e) Best performance for molybdenum coatings

shown that the asperity contact and the EHL film share the load (Ref 86). According to Ref 87, these asperity contacts produce high stress concentrations very close to the surface but do not change the subsurface Hertzian stress pattern. These stress concentrations due to the interaction of asperities in the presence of microslip within the contact region result in shear stress beneath the asperity. Hard coatings such as WC-Co and Al_2O_3 respond to this stress concentration by microcracking and eventual micropitting, which also results in the attenuation of near-surface compressive residual stress within the coating material (Ref 88).

Apart from the mechanism of asperity interactions and subsequent microcracking leading to abrasive failure in TS coatings, the criterion of maximum tensile stress at the edge of the contact area for brittle materials is also thought to be responsible for the abrasive wear of TS cermet and ceramic coatings. The tensile stress is very sharply localized and decays very rapidly at small depths below the surface. For elliptical contacts, this tensile stress (T_{max}) for a given value of peak compressive stress (P_o) can be evaluated from the following relation, reproduced here for clarity (Ref 32, 33).

$$\frac{T_{max}}{P_o} = \frac{0.33 \times \beta}{n^3}\left[0.5 \ln\left(\frac{1+n}{1-n}\right) - n\right] \quad \text{(Eq 8)}$$

where β is the ratio of minor to major axes of contact ellipse, and $n = (1 - \beta^2)^{0.5}$. For most of the RCF test conditions listed in Table 4, for example, in a rolling four-ball machine, T_{max} can be approximated as 324 MPa (47 ksi), for example, at a compressive contact stress of 2.7 GPa (0.39×10^6 psi). The fracture stress of WC-Co coatings (using the tensile test technique) has been shown to be in the range of 380–690 MPa (55–100 ksi) for high-velocity plasma sprayed and D-gun coatings (Ref 89). These values of fracture stress are similar to the tensile stresses associated with the Hertzian stress distribution at the edge of the contact region. This indicates that even under a fully developed EHL ($\lambda > 3$) regime, the microcracks in the coating material, either due to coating defects or asperity contact, can propagate due to tensile stress at the edge of the contact area. Hence, coating fracture toughness, which is related to coating microstructure via various TS processes and process conditions, is critical in controlling abrasive failure; for example, Ahmed and Hadfield (Ref 84) have related the poor fracture toughness of APS coatings in comparison to the liquid-fuel HVOF system, with the higher rate of abrasive wear in APS coatings.

Delamination Failure in TS Coatings. Suh initially proposed a delamination theory of sliding wear in 1973 (Ref 2). Flemming and Suh (Ref 90), Suh and Saka (Ref 91), and Suh (Ref 92) have since performed experimental and theoretical analysis supporting the delamination theory. The mechanism of delamination wear includes the propagation of cracks parallel to the surface at a depth governed by material properties and the friction coefficient. Although rolling friction prevails in RCF tests and the delamination theory of wear is based on sliding friction, nevertheless the similarities of the failure mechanism in both cases are compelling. Typical observation of coating delamination at the coating-substrate interface can be seen from Fig. 12 for Al_2O_3 coating, whereas the delamination failure within the coating material can be appreciated from Fig. 13 for WC-Co coating. Coatings of Al_2O_3, however, have not shown delamination within the coating material but only at the coating-substrate interface (Table 4). Sheetlike debris that reached a few millimeters in major dimension is produced during this process.

Mechanism of Coating Delamination in Cermet and Ceramic Coatings. The damage theory of materials begins with the premise that material contains a multitude of defects in the form of microvoids (Ref 93) that undergo extension due to loading and unloading. A similar approach is adapted to explain the mechanism of coating delamination. A TS coating microstructure contains varying levels of micropores, microcracks, and secondary-phase particles, which act as stress concentration during cyclic loading. The extent of these microdefects varies for different coating techniques and also depends on the starting powder, coating process, and its parameters. Such is the complexity of microstructure that stress concentrations are inevitable during cyclic loading. During rolling contact, these microdefects have a higher tendency for crack propagation at the depths of maximum shear stress (τ_{max}) and orthogonal shear stress reversal

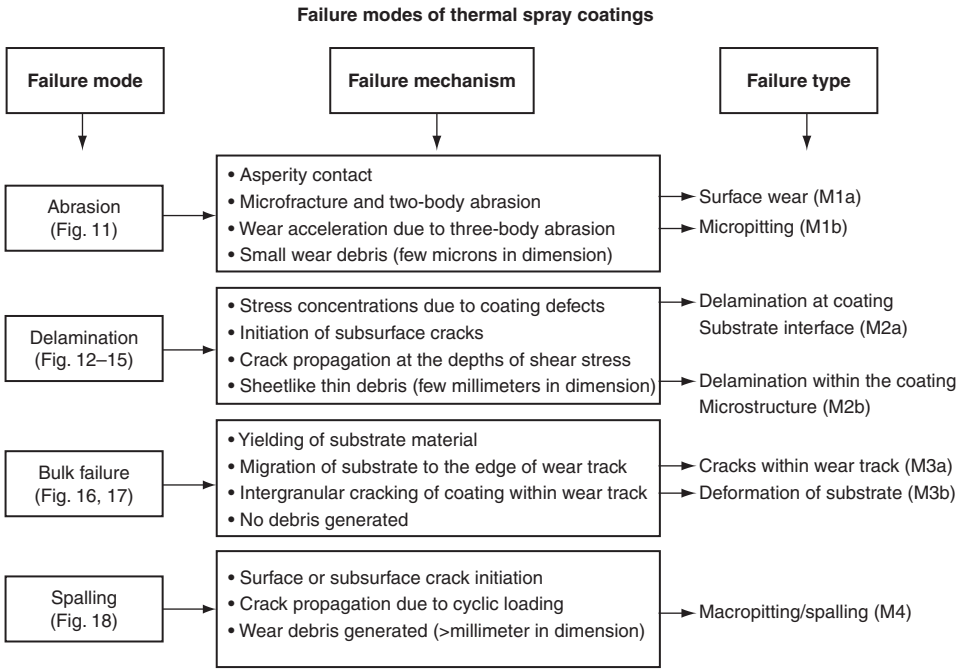

Fig. 10 Rolling-contact fatigue failure modes of thermal spray cermet and ceramic coatings. Source: Ref 84

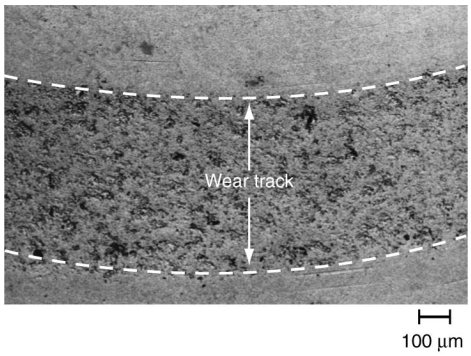

Fig. 11 Abrasive failure of the rolling wear track in thermally sprayed WC-Co coating

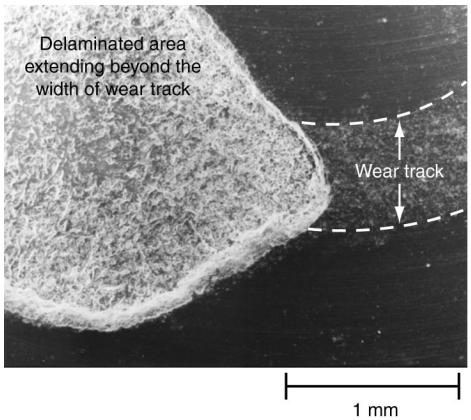

Fig. 12 Adhesive delamination in thermally sprayed Al_2O_3 coating

(τ_{orth}) (Fig. 8). The location of these stresses in the vicinity of the coating-substrate interface can thus significantly influence crack propagation due to the mismatch of coating and substrate properties and a high level of quenching stress at this interface (Ref 94). Circumferencial cracks similar to those shown in Fig. 14 appear beneath the surface at the depths of maximum shear and orthogonal shear stress for WC-Co coatings, whereas in the case of Al_2O_3 coatings, cracks generally appear at the coating-substrate interface. Hence, cohesive and adhesive delamination is observed in cermets whereas adhesive delamination is the preferred failure mode in ceramic coatings.

Figure 15 gives a schematic of crack propagation behavior in ceramic and cermet coatings. The process can be summarized as follows:

- Crack initiation: For cermet (WC-Co) coatings, cracks initiate subsurface at different depths under the contact region but propagate at the depths of maximum shear stress and orthogonal shear stress (Fig. 14a). These cracks initiate due to stress concentrations in the presence of microstructural defects. For WC-Co coatings thinner than the depth of maximum shear stress, an additional factor of stress concentrations is the mismatch of coating-substrate properties at the interface. For WC-Co coatings thicker than the depth of maximum shear stress, these cracks initiate within the coating microstructure; for coatings thinner than the depth of maximum shear stress, these cracks initiate within the coating microstructure as well as at the coating-substrate interface. For ceramic (Al_2O_3) coatings, cracks generally initiate at the coating-substrate interface.
- Crack propagation: For WC-Co coatings thicker than the depth of maximum shear stress, initiated cracks propagate slowly in response to cyclic loading at their respective depths within the coating microstructure (Fig. 14b). For WC-Co or ceramic (Al_2O_3) coatings thinner than the depth of maximum shear stress, the cracks at the coating-substrate interface propagate much faster than the cracks at the depth of orthogonal shear stress (i.e., cracks within the coating microstructure) and result in poor RCF performance of thinner coatings.
- Crack extension: For WC-Co coatings thicker than the depth of maximum shear stress, the cracks at maximum shear stress extend to greater lengths and ultimately join the cracks at the depth of orthogonal shear stress (Fig. 14b). For coatings thinner than the depth of maximum shear stress or for ceramic (Al_2O_3)

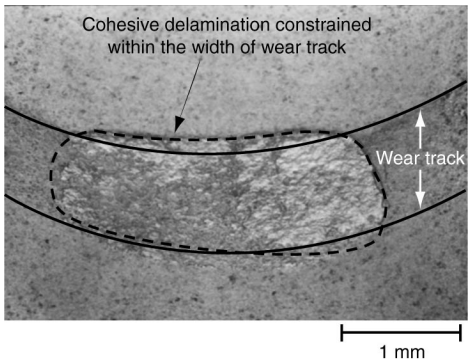

Fig. 13 Cohesive delamination in thermally sprayed WC-Co coating (backscattered electron image)

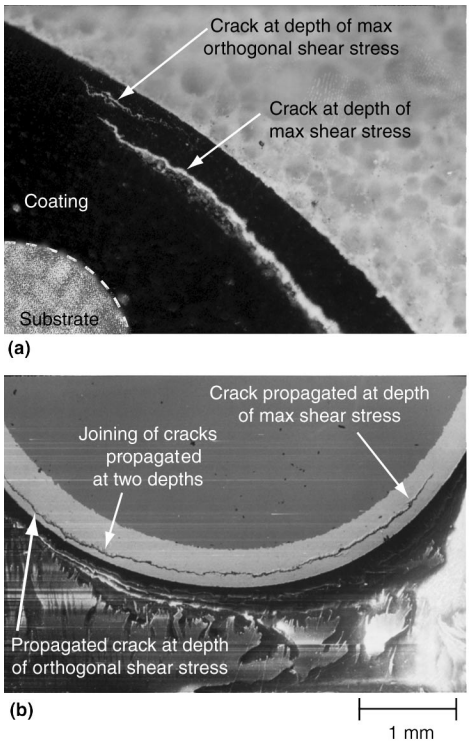

Fig. 14 Subsurface crack observations during delamination failure of thermal spray coatings. (a) Subsurface cracks in WC-Co-coated rolling cone at the depths of maximum and orthogonal shear stress. (b) Propagated subsurface cracks leading to coating delamination during RCF failure of WC-Co coating

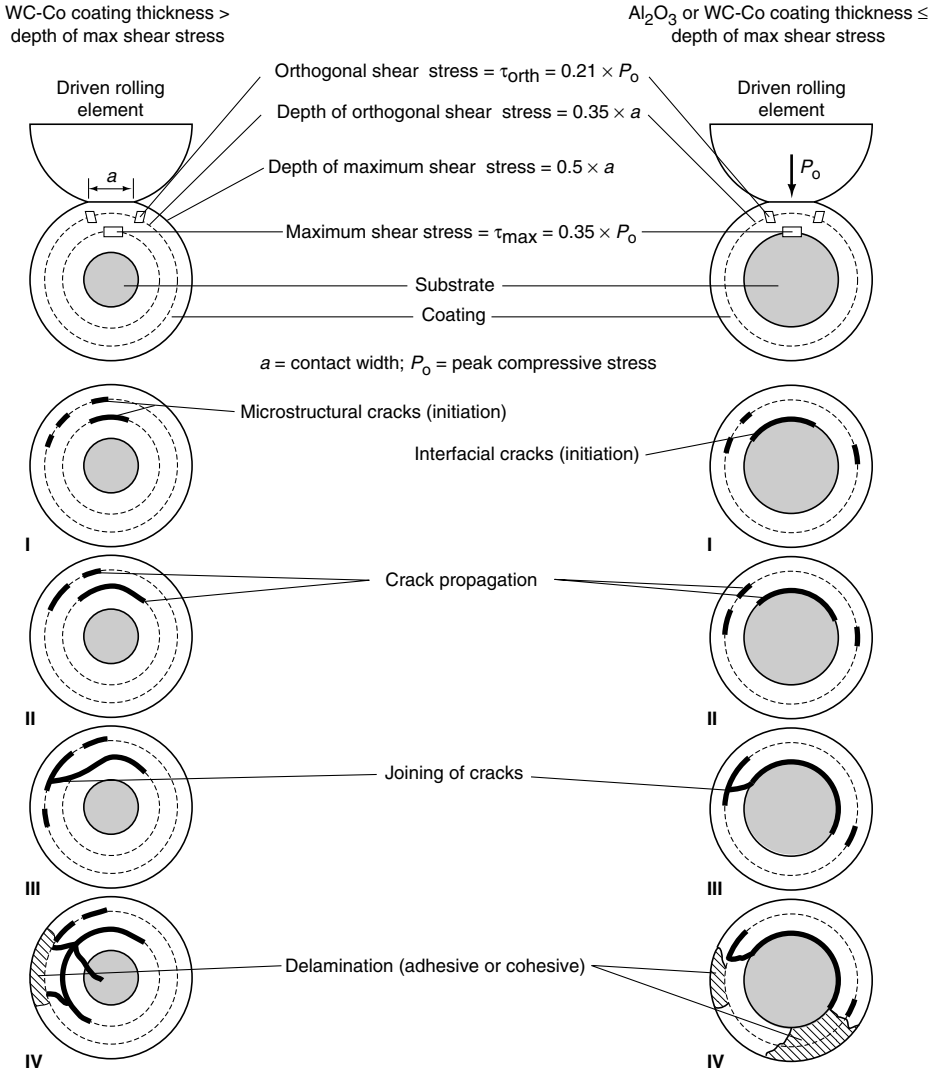

Fig. 15 Schematic of coating delamination process for cermet and ceramic coatings

coatings, the cracks at interface had the greater tendency of reaching the surface independently, and, in some cases, they combine with the cracks at the depth of orthogonal shear stress and eventually reach the surface.

- Delamination: For WC-Co coatings thicker than the depth of maximum shear stress, the cracks from the depth of orthogonal shear stress reach the surface much more quickly than the cracks at the depth of orthogonal shear stress, thereby leading to coating delamination at the depth of orthogonal shear stress. Contrary to this, for thinner WC-Co or ceramic (Al_2O_3) coatings, interfacial delamination takes place.

Coating Failure Due to Bulk Deformation. Bulk deformation of substrate material is of primary importance for the cases of hard coatings (WC-Co and Al_2O_3) on a soft substrate. This is because the contact stress can be in the elastic range of the coating material and in the plastic range of the substrate. The primary effect of this is the plastic flow of substrate, leading to conformity of the contact region and a hump at the edge of the wear track. Figure 16 shows a typical example of such a failure in which the substrate could no longer support the coating, leading to bending and cracking of coating material in the initial stages of RCF failure. As cyclic loading continues, the coating cracks in the middle of the wear track due to its inability to plastically deform under the tensile stress caused by the plastic flow of substrate material. During this failure, the plastic flow of the substrate continues, and the substrate is pushed up at the edges of the wear track as it conforms to the geometry of the counterbody, leading to subsequent cracking at the edge of the wear track. Further cyclic loading leads to crack propagation in tension, and the substrate finally emerges at the edge of wear track. Because the crack propagation is progressive due to cyclic loading, this failure mode is categorized as a RCF failure mode. Once the conformity of contact is such that the stresses in the substrate are no longer in the plastic region, the substrate migration terminates, and a steady state is reached. Figure 17 shows a schematic of this failure mode and indicates that substrate hardness should be carefully selected (based on contact loading) to combat this failure. The mechanism of bulk deformation is thus strongly dependent on the ability of the substrate material to support the coating in relation to the contact stress and is marginally affected by the changes in either coating material or process.

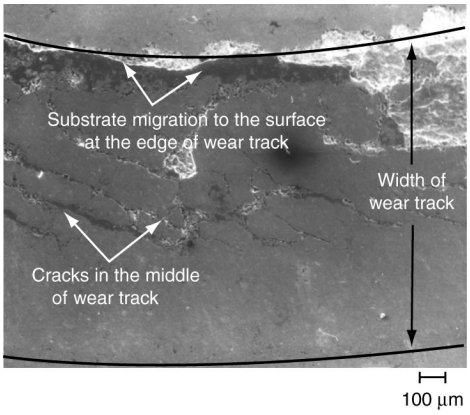

Fig. 16 Bulk deformation failure of WC-Co coating, indicating cracks in the middle of the wear track and substrate migration at the edge of the wear track

Coating Failure Due to Spalling. Spalling is the most commonly seen RCF failure in steel rolling-element bearings. Spalling fatigue is, however, the most rare mode of fatigue failure in TS coatings. Spall in TS coatings resembles in appearance the spalls in conventional bearings, as shown in Fig. 18. It differs from delamination failure (discussed previously) in the sense that spall is contained within the wear track and is circular or elliptical in appearance, with its surface area (or width-to-depth ratio) much smaller than that of delaminated coating. A comparison of Fig. 1,12 and 18 can distinguish the appearance between the two failures. As with conventional steel bearings, spalls in TS coatings can initiate from micropits, furrows, grinding marks, or dents on the surface of a wear track. Also, subsurface inclusions and defects are known to lead to spalling of rolling elements. Examination of the wear track of a spalled specimen in TS coatings indicates that substantial micropitting of the wear track occurs before fatigue spall is produced. This highlights the possibility that the fatigue spall in TS coatings initiates from the micropits, and subsequent crack propagation takes place due to cyclic loading. It is also possible that once initiated, spalling can be assisted by hydraulic pressure crack propagation (Ref 4). However, the exact mechanism of fatigue spall, that is, surface or subsurface initiation and propagation, in TS coatings is not completely understood at this stage.

Design Considerations for RCF Applications of TS Coatings. The design of surface overlay coatings for tribological applications involving Hertzian contact loading not only requires a thorough understanding of the tribological conditions, for example, contact stress, lubrication, and friction, but also the influence of coating processes, material, thickness, and the role of substrate material properties. Tribologists often have little choice about the former but can influence the coating performance by appropriate selection of the latter. The following thus provides some insight into the design considerations of coating-substrate material properties, coating thickness, and coating processes to combat RCF failure in TS coatings.

Substrate Material. The mechanism of bulk and interfacial delamination failure mode (discussed above) indicated that the four most important design considerations while selecting the substrate material are:

- Ability to support the coating
- Higher coefficient of thermal expansion than the coating material, to induce a certain degree of compressive residual stress within the coating material
- Ability to withstand preheat temperature prior to thermal spraying
- Ability to plastically deform during shot peening prior to the coating process, to pro-

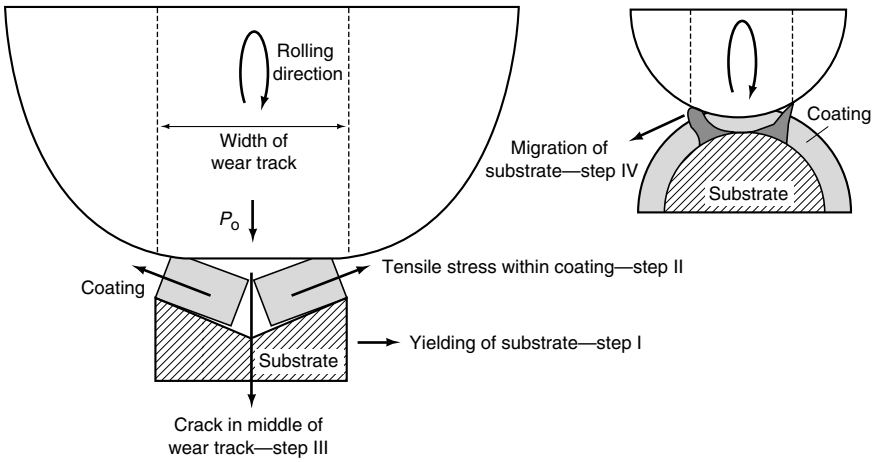

Fig. 17 Mechanism of bulk deformation

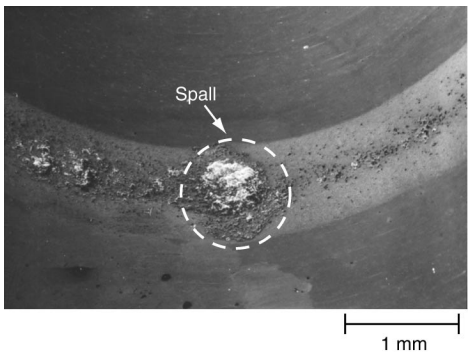

Fig. 18 Spalling of thermally sprayed WC-Co coating

mote mechanical interlock at the coating-substrate interface

The ratio ($\delta = P_o/\sigma$, where δ is normalized pressure) of the Hertzian contact stress (P_o) to the substrate yield strength (σ) is thus a useful indicator in determining the ability of the substrate to support the coating. Figure 19 shows this effect and indicates that normalized contact stress (P_o/σ) can be used to benchmark candidate substrate materials.

Coating Thickness. Investigations of the delamination failure mode (both cohesive and adhesive) indicated that while selecting the coating thickness for a given coating-substrate system, it is critical to shift the maximum and orthogonal shear stresses away from the coating substrate interface. Using this technique can also simplify the coating design by not having to functionally grade the material to avoid the sharp stress gradient at the interface during the Hertzian loading. Hence, the ratio ($\Delta = \xi/\Psi$, where Δ is the normalized coating thickness, ξ is the average coating thickness, and Ψ is the depth of maximum shear stress) of the coating thickness to the depth of shear stress ($\Psi = 0.65b$, where b is the length of the minor axis of the contact ellipse) is found to be a good indicator of the coating substrate system to combat adhesive delamination. Figure 20 shows this effect and indicates that Δ value can have a significant influence on the fatigue performance of coatings.

Coating Material. Investigation of failure modes in TS coatings indicated that the selection of a hard, wear-resistant coating material requires a consideration of its coefficient of thermal expansion and the ability of the coating process to produce a dense coating microstructure. Within the boundaries of materials considered in published research (WC-Co and Al_2O_3), test results indicate that the cermet coatings performance was superior to that of the ceramic coatings. This was mainly because of the following three reasons:

- The lower melting point of cermet material the allowed the melting of lamellas during the HVOF processes, whereas ceramic was partially melted, resulting in a lower cohesive and adhesive strength.
- Although higher temperatures during the APS process melted the ceramic particles, the velocities achieved are generally much lower than the HVOF system, resulting in porous microstructure and thus lower strength.
- A higher lamella temperature during the APS process would have a high rate of cooling (quenching) on impact with the underlying surface, which can lead to internal cracking.

These factors contributed toward lower adhesive and cohesive strength of ceramic coatings and indicate the need for an interfacial layer. With the advancements of high-velocity plasma systems, however, it may be possible to improve RCF of TS ceramics in the future.

Coating Process(es). The most important consideration while selecting the coating process for RCF applications is its ability to produce a dense coating microstructure, resulting in a higher mechanical strength. There are a number of ways to analyze this, for example, porosity measurements, x-ray diffraction pattern, microhardness and bond strength. Experimental research has indicated that a useful measure for RCF applications is to compare the indentation fracture toughness (K_{Ic}) of the coating material. So far, HVOF-deposited WC-Co coatings with $K_{Ic} \geq 1.7$ MPa$\sqrt{m}$ have shown a fatigue life in excess of 70 million stress cycles for coating design parameters of $\Delta \geq 1.5$ and $\delta \leq 1.5$ (e.g., Ref 84).

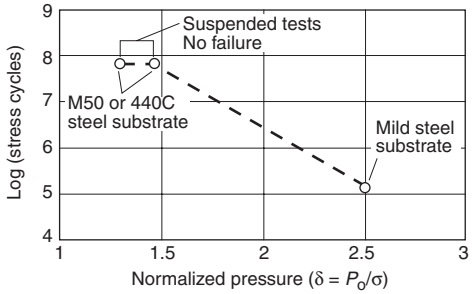

Fig. 19 Influence of normalized pressure on stress cycles ($\Delta \geq 1.5$, $P_o = 2.7$ GPa, or 0.39×10^6 psi)

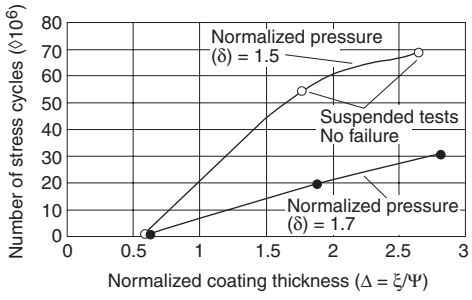

Fig. 20 Influence of normalized coating thickness on the performance of HVOF coating on 440C steel substrate ($\sigma = 1840$ MPa, or 267 ksi)

REFERENCES

1. N.P. Suh, An overview of the Delamination Theory of Wear, *Wear,* Vol 44, 1977, p 1–16
2. N.P. Suh, The Delamination Theory of Wear, *Wear,* Vol 25, 1973, p 111–124
3. D. Tabor, The Mechanism of Rolling Friction, Part II: The Elastic Range, *Proc. R. Soc. A,* Vol 229, 1955, p 198–220
4. S. Way, Pitting Due to Rolling Contact, *J. Appl. Mech.,* 1935, p A49–A58
5. T.E. Tallian, On Competing Failure Modes in Rolling Contact, *ASLE Trans.,* Vol 10, 1967, p 418–439
6. M. Hadfield, T.A. Stolarski, and R.T. Cundill, Failure Modes of Ceramics in Rolling Contact, *Proc. R. Soc. A,* Vol 443, 1993, p 607–621
7. R. Ahmed and M. Hadfield, Failure Modes of Plasma Sprayed WC-Co Coated Rolling Elements, *Wear,* Vol 230, 1999, p 39–55
8. J.V. Poplawski, S.M. Peters, and E.V. Zaretsky, Effect of Roller Profile on Cylindrical Roller Bearing Life, Part I: Comparison of Bearing Life Theories, *Tribol. Trans.,* Vol 44 (No. 3), 2001, p 339–350
9. T.E. Tallian, Data Fitted Bearing Life Prediction Model for Variable Operating Conditions, *Tribol. Trans.,* Vol 42 (No. 1), 1999, p 241–249
10. Y. Li, T.R. Kurfess, and S.Y. Liang, Stochastic Prognostics for Rolling Element Bearings, *Mech. Syst. Signal Process.,* Vol 14 (No. 5), 2000, p 747–762
11. R.S. Hyde, Contact Fatigue of Hardened Steels, *Fatigue and Fracture,* Vol 19, *ASM Handbook,* 1996, p 680–690
12. W.A. Glaeser and S.J. Shaffer, Contact Fatigue, *Fatigue and Fracture,* Vol 19, *ASM Handbook,* 1996, p 331–336
13. P.J. Blau, Rolling Contact Wear, *Friction, Lubrication, and Wear Technology,* Vol 18, *ASM Handbook,* 1992, p 257–262
14. W.D. Syniuta and C.J. Corrow, A Scanning Electron Microscope Fractographic Study of Rolling Contact Fatigue, *Wear,* Vol 15, 1970, p 187–199
15. J.A. Martin and A.D. Eberhardt, Identification of Potential Failure Nuclei in Rolling Contact Fatigue, *J. Basic Eng.* (Trans. ASME), 1967, p 932–942
16. W.E. Littmann and R.L. Widner, Propagation of Contact Fatigue from Surface and Subsurface Origins, *J. Basic Eng.* (Trans. ASME), 1966, p 624–636
17. W.E. Littmann, The Mechanism of Contact Fatigue, Conf. Proc. *An Interdisciplinary Approach to the Lubrication of Concentrated Contacts,* National Aeronautics and Space Administration, 1969, p 309–377
18. E.V. Zaretsky, "Life Factors for Rolling Bearings," Society of Tribology and Lubrication Engineers (STLE) publication, 1999
19. R.A. Guyer, *Rolling Bearings Handbook and Trouble Shooting Guide,* CRC Press, 1996
20. T. Harris, *Rolling Bearing Analysis,* 3rd ed., John Wiley & Sons, 1991
21. Anon, Friction, Wear, and Lubrication Terms and Definitions, 1st revision, Organization for Economic Co-Operation and Development, Paris, 1968
22. F.J. Wren and C.A. Moyer, Modes of Fatigue Failures in Rolling Element Bearings, *Proc. Inst. Mech. Eng.,* Vol 179 (Part 3D), 1964-1965, p 236–247
23. Y.P. Chiu, T.E. Tallian, and J.I. McCool, An Engineering Model of Spalling Fatigue in Rolling Contact—The Subsurface Model, *Wear,* Vol 17, 1971, p 433–446
24. T.E. Tallian and J.I. McCool, An Engineering Model of Spalling Fatigue in Rolling Contact—The Surface Model and Engineering Discussion and Illustrative Examples, *Wear,* Vol 17, 1971, p 447–480

25. T.E. Tallian, *Failure Atlas for Hertz Contact Machine Elements,* 2nd ed. ASME Press, 1999
26. J.J.C. Hoo, "Rolling Contact Fatigue Testing of Bearing Steels," STP 771, ASTM, 1982
27. L.D. Wedeven, R.A. Pallini, and C.G. Hingley, "Selection and Use of Wear Tests for Ceramics," STP 1010, ASTM, 1988, p 58–73
28. R. Tourret and E.P. Wright, *Rolling Contact Fatigue: Performance Testing of Lubricants,* Int. Symp., Inst. of Petroleum, Heyden and Sons, London, 1977
29. W. Cheng, W.S. Cheng, and L.M. Keer, Experimental Investigation on Rolling Sliding Contact Fatigue Crack Initiation with Artificial Defects, Tribol. Trans., Vol. 37, 1994
30. G. Xu, F. Sadeghi, and M.R. Hoeprich, Dent Initiated Spall Formation in EHL Rolling/Sliding Contact, *J. Tribology (Trans. ASME),* Vol 120, 1998, p 453–462
31. Engineering Science Data Unit, "Contact Phenomena, Part I: Stresses, Deflections and Contact Dimensions for Normally-Loaded Unlubricated Elastic Components," ESDU 78035, Inst. of Mech. Eng., 1984
32. Engineering Science Data Unit, "Contact Phenomena, Part II: Stress Fields and Failure Criteria in Concentrated Elastic Contacts under Combined Normal and Tangential Loading," ESDU 84017, Inst. of Mech. Eng., 1984
33. G. Lundberg and A. Palmgren, Dynamic Capacity of Rolling Bearings," *Acta Polytech. Scand.,* Vol 1 (No. 3), 1947
34. N.G. Popinceanu, E. Diaconescu, and S. Cretu, Critical Stresses in Rolling Contact Fatigue, *Wear,* Vol 71, 1981, p 265–282, 1981
35. W.J. Anderson and E.V. Zaretsky, Rolling Element Bearings—A Review of the State of the Art, NASA TMX-71441, National Aeronautics and Space Administration, Cleveland, OH, 1973
36. T.A. Harris, Friction and Wear of Rolling-Element Bearings, *Friction, Lubrication, and Wear Technology,* Vol 18, *ASM Handbook,* 1992, p 499–514
37. A. Kapoor and J.A. Williams, Shakedown Limits in Sliding Contacts on a Surface-Hardened Half-Space, *Wear,* Vol 172, 1994, p 197–206
38. A. Kapoor and K.L. Johnson, Effects on Changes in Contact Geometry on Shakedown of Surfaces in Rolling Sliding Contact, *Int. J. Mech. Sci.,* Vol 34 (No. 3), 1992, p 223–239
39. O. Orringer, W.R. Paxton, D.E. Gray, and P.K. Raj, Residual Stress and Its Consequences on Both Sides of the Wheel-Rail Interface, *Wear,* Vol 191, 1996, p 25–34
40. Q. Chen, G.T. Hahn, C.A. Rubin, and V. Bhargava, The Influence of Residual Stresses on Rolling Contact Mode II Driving Force in Bearing Raceways, *Wear,* Vol 126, 1988, p 17–30
41. H. Muro, N. Tsushima, and K. Nunome, Failure Analysis of Rolling Bearings by X-Ray Measurement of Residual Stress, *Wear,* Vol 25, 1973, p 345–356
42. R.J. Pomeroy, Measurement of Residual Stress in Rolling Contact, *Wear,* Vol 16, 1970, p 393–412
43. A. Igartua, J. Laucircia, A. Aranzabe, T. Leyendecker, O. Lemmer, G. Erkens, M. Weck, and G. Hanrath, Application of Low Temperature PVD Coatings in Roller Bearings: Tribological Tests and Experiences with Spindle Bearing Systems, *Surf. Coat. Technol.,* Vol 86–87, 1996, p 460–466
44. A. Erdemir, Rolling Contact Fatigue and Wear Resistance of Hard Coatings on Bearing Steel Substrates, *Surf. Coat. Technol.,* Vol 54–55, 1992, p 482–489
45. K.D. Bouzakis, N. Vidakis, A. Lontos, S. Mitsi, and K. David, Implementation of Low Temperature-Deposited Coating Fatigue Parameters in Commercial Roller Bearings Catalogues, *Surf. Coat. Technol.,* Vol 133–134, 2000, p 489–496
46. K.D. Bouzakis, N. Vidakis, and S. Mitsi, Fatigue Prediction of Thin Hard Coatings on the Steel Races of Hybrid Bearings Used in High Speed Machine Tool Spindles, *J. Tribology, (Trans. ASME),* Vol 120, 1998, p 835–842
47. I.A. Polonsky, T.P. Chang, L.M. Keer, and W.D. Sproul, An Analysis of the Effect of Hard Coatings on Near-Surface Rolling Contact Fatigue Initiation Induced by Surface Roughness, *Wear,* Vol 208, 1997, p 204–219
48. K. Holmberg and A. Matthews, *Coatings Tribology: Properties, Techniques, and Applications in Surface Engineering, Tribology Series,* Vol 28, Elsevier Science, 1994
49. L. Pawlowski, The Science and Engineering of Thermal Spray Coatings, John Wiley & Sons, 1995
50. N.J.M. Carvalho, A.J. Huis in't Veld, and J.T. De Hossen, Interfacial Fatigue Stress in PVD TiN Coated Tool Steels Under Rolling Contact Fatigue Conditions, *Surf, Coat, Technol.,* Vol 105, 1998, p 109–116
51. I.A. Polonsky, T.P. Chang, L.M. Keer, and W.D. Sproul, A Study of Rolling-Contact Fatigue of Bearing Steel Coated with Physical Vapor Deposition TiN films: Coating Response to Cyclic Contact Stress and Physical Mechanisms Underlying Coating Effect on the Fatigue Life, *Wear,* Vol 215, 1998, p 191–204
52. G. Meier zu Kocker, E. Santner, and B. Loffelbein, Functional Behavior of PVD Coatings under Sliding and Rolling Stress Conditions, *Tribotest J.,* Vol 4 (No. 3), 1998, p 241–260
53. R. Thom, L. Moore, W.D. Sproul, and T.P. Chang, Rolling Contact Fatigue Tests of Reactively Sputtered Nitride Coatings of Ti, Zr, Hf, Mo, Ti-Al, Ti-Zr, Ti-Al-V on 440C Stainless Steel Substrates, *Surf. Coat. Technol.,* Vol 62, 1993, p 423–427
54. T.P. Chang, P. Taung-Sea, H.S. Cheng, and S. Herbert, Influence of Coating Thickness on Lubricated Rolling Contact Fatigue Life, *Surf. Coat. Technol.,* Vol 44 (No. 1–3), 1990, p 699–708
55. T.P. Chang, H.S. Cheng, H.S. Chiou, and W.D. Sproul, Comparison of Fatigue Life Morphology between TiN Coated and Uncoated Rollers, *Tribol. Trans.,* Vol 34 (No. 3), 1991, p 408–416
56. P.J. Rudnik and W.D. Sproul, "Ceramic Coated Bearing Elements for Improved Durability and Reliability," final report, Project F33615-92-C-5295, Advanced Research Projects Agency (APRA), 1994
57. M.A. Liston, Rolling Contact Fatigue Properties of TiN/NbN Superlattice Coatings on M-50 Steel, *ASTM Spec. Tech. Publ.,* Vol 1327, 1998, p 499–510
58. R. Wei, P.J. Wilbur, M. Liston, and G. Lux, Rolling Contact Fatigue Wear Characteristics of Diamond-Like Carbon Coatings on Steels, *Wear,* Vol 162–164, 1993, p 558–568
59. R. Wei, P.J. Wilbur, and F.M. Kustas, A Rolling Contact Fatigue Study of Hard Carbon Coated M-50 Steel, *Trans ASME,* Vol 114, 1992, p 298–302
60. L. Rosado, V.K. Jain, and H.K. Trivedi, The Effect of Diamond-Like Carbon Coatings on the Rolling Fatigue and Wear of M-50 Steel, *Wear,* Vol 212, 1997, p1–6
61. A.J. Perry, M. Jagner, W.D. Sproul, and P.J. Rudnik, Residual Stress and Strain Distribution Anomalies in TiN Films Deposited by Physical Vapour Deposition, *Surf. Coat. Technol.,* Vol 42 (No. 1), 1990, p 49–68
62. I. Petrov, L. Hultman, U. Helmersson, and J.E. Sundgren, Microstructure Modification of TiN by Ion Bombardment during Reactive Sputter Deposition, *Thin Solid Films,* Vol 169, 1989, p 299–314
63. K.D. Bouzakis, N. Vidakis, A. Igartua, T. Leyendecker, G. Erkens, M. Weck, G. Hanrath, and A. Schumacher, "Application of Low Temperature PVD Coatings in Roller Bearings-Fatigue Prediction of Thin Hard Coatings—Tribological Tests and Experiments with Spindle Bearing Systems," final report of the BRITE project Eurobearings, European Commission technical report, BRE-CT92-0333, 1997
64. H. Djabella and R.D. Arnell, Finite Element Analysis of Contact Stress in Elastic Coating on an Elastic Substrate, *Thin Solid Films,* Vol 213, 1992, p 205–209
65. P.K. Gupta and J.A. Walowit, Contact Stress between an Elastic Cylinder and a Layered Elastic Solid, *Trans. ASME,* 1974, p 250–257
66. A. Otsuka, H. Sugawara, and M. Shomura, A Test Method for Mode-II Fatigue Crack Growth Relating to a Model for Rolling Contact Fatigue, *Fatigue Fract. Eng. Mater. Struct.,* Vol 19, 1996, p 1265–1275

67. M. Hadfield and T.A. Stolarski, The Effect of the Test Machine on the Failure Mode in Lubricated Rolling Contact of Silicon Nitride, *Tribol. Int.,* Vol 28, 1995, p 377–382
68. J. He, C. Bai, K. Xu, and N. Hu, Improving the Anticorrosion and Mechanical Behaviour of PACVD TiN, *Surf. Coat. Technol.,* Vol 74–75, 1995, p 387–393
69. J. He, K. Xu, and N. Hu, Evaluation of Bonding Strength of Thin Hard Films by Spherical Rolling Test, *Surf. Coat. Technol.,* Vol 97, 1997, p 295–298
70. K. Xu, N. Hu, and J. He, Evaluation of the Bond Strength of Hard Coatings by the Contact Fatigue Test, *J. Adhes. Sci. Technol.,* Vol 12, 1998, p 1055–1069
71. J.F. Dill, M.N. Gardos, H.E. Hintermann, and H.J. Boving, Rolling Contact Fatigue Evaluation of Hardcoated Bearing Steels, *ASCE Publ.,* 1984, p 230–240
72. L. Chao, R. Lakshminarayanan, D.K. Shetty, and R. Cutler, Rolling Contact Fatigue and Wear of CVD SiC with Residual Surface Compression, *J. Am. Ceram. Soc.,* Vol 78 (No. 9) 1995, p 2307–2313
73. A. Savan, H.J. Boving, F. Fluehmann, and H.E. Hintermann, Increased Performance of Bearings Using TiC-Coated Balls, *J. Phys. (France) IV,* Colloque C7, Supplement au *J. Phys. (France) III,* Vol 3, Nov 1993, p 943–947
74. R. Nieminen, P. Vouristo, K. Niemi, T. Mantyla, and G. Barbezat, Rolling Contact Fatigue Failure Mechanisms in Plasma and HVOF Sprayed WC-Co Coatings, *Wear,* Vol 212, 1997, p 66–77
75. M. Yoshida, K. Tani, A. Nakahira, A. Nakajima, and T. Mawatari, Durability and Tribological Properties of Thermally Sprayed WC Cermet Coatings in Rolling/Sliding Contact, *Proc. ITSC,* May 1995 (Kobe), p 663–668
76. R. Ahmed and M. Hadfield, Rolling Contact Fatigue Performance of Detonation Gun Coated Elements, *Tribol. Int.,* Vol 30, 1997, p 129–137
77. R.Ahmed, M. Hadfield, Rolling Contact Fatigue Behaviour of Thermally Sprayed Rolling Elements, *Surf. Coat. Technol.,* Vol 82, 1996, p176–186
78. B.Y. Sarma and M.M. Mayuram, Some Studies on Life Prediction of Thermal Sprayed Coatings under Rolling Contact Conditions, *J. Tribology (Trans ASME),* Vol 122, 2000, p 503–510
79. A. Nakajima, T. Mawatari, M. Yoshida, K. Tani, and A. Nakahira, Effects of Coating Thickness and Slip Ratio on Durability of Thermally Sprayed WC Cermet Coatings in Rolling/Sliding Contact, *Wear,* Vol 241, 2000, p 166–173
80. A. Makela, P. Vouristo, M. Lahdensuo, K. Niemi, and T. Mantyla, Rolling Contact Fatigue Testing of Thermally Sprayed Coatings, *Proc. Seventh Int. Thermal Spray Conf.,* 20–24 June 1994 (Boston, MA), ASM International, 1994, p 759–763
81. R. Ahmed and M. Hadfield, Wear of High-Velocity Oxy-Fuel (HVOF)-Coated Cones in Rolling Contact, *Wear,* Vol 203–204, 1997, p 98–106
82. R. Ahmed, M. Hadfield, Influence of Coating Thickness and Contact Stress on the Fatigue Failure of HVOF Coatings, *Int. Thermal Spray Conf.,* (Singapore), ASM International, 2001, p 1009–1015
83. S. Tobe, S. Kodama, and H. Misawa, Rolling Fatigue Behaviour of Plasma Sprayed Coatings on Aluminum Alloy, *Proc. Nat. Thermal Spray Conf.* 1990 (Tokyo, Japan), ASM International, 1990, p 171–178
84. R. Ahmed and M. Hadfield, Mechanisms of Fatigue Failure in Thermal Spray Coatings, *J. Therm. Spray Technol.,* in press 2002
85. R. Ahmed, Contact Fatigue Failure Modes of HVOF Coatings, *Wear,* submitted for publication 2001
86. K.L. Johnson, J.A. Greenwood, and S.Y. Poon, A Simple Theory of Asperity Contact in Elastohydrodynamic Lubrication, *Wear,* Vol 19, 1972, p 91–108
87. D. Berthe, L. Flamand, and M. Godet, Micropitting in Hertzian Contacts, *J. Lubr. Technol.,* (*Trans. ASME*), Vol 102, 1980, p 479–485
88. R. Ahmed and M. Hadfield, Experimental Measurement of Residual Stress Field within Thermally Sprayed Rolling Elements, *Wear,* Vol 209, 1997, p 84–95
89. R.C. Tucker, Jr., Structure Property Relationship in Deposits Produced by Plasma Spray and Detonation Gun Techniques, *J. Vac. Sci. Technol.,* Vol 11, 1994, p 725–734
90. J.W. Flemming and N.P. Suh, Mechanics of Crack Propagation in Delamination Wear, *Wear,* Vol 44, 1977, p 39–56
91. N.P. Suh and N. Saka, Fundamentals of Tribology, *Int. Conf. Fundamentals of Tribology,* Massachusetts Institute of Technology Press, 1980
92. N.P. Suh, *Tribophysics,* Prentice Hall, 1986
93. P.J. RabIer, Some Remarks on Damage Theory, *Int. J. Eng. Sci.,* Vol 27, 1989, p 29–54
94. S.C. Gill, "Residual Stress in Plasma Sprayed Deposits," Ph.D. dissertation, Gonville and Caius College, Cambridge, U.K., 1993